Coupled thermo-hydro-mechanical calculations of the water saturation phase of a KBS-3 deposition hole

Influence of hydraulic rock properties on the water saturation phase

Lennart Börgesson
Clay Technology AB

Jan Hernelind
FEM-Tech AB

December 1999

Coupled thermo-hydro-mechanical calculations of the water saturation phase of a KBS-3 deposition hole

Influence of hydraulic rock properties on the water saturation phase

Lennart Börgesson
Clay Technology AB

Jan Hernelind
FEM-Tech AB

December 1999

Abstract

The wetting process in deposition holes designed according to the KBS3-concept has been simulated with finite element calculations of the thermo-hydro-mechanical processes in the buffer, backfill and surrounding rock. The buffer material has been modelled according to the preliminary material models developed for swelling clay.

The properties of the rock have been varied in order to investigate the influence of the rock properties and the hydraulic conditions on the wetting processes. In the modelling of the test holes the permeability of the rock matrix, the water supply from the backfill, the water pressure in the surrounding rock, the permeability of the disturbed zone around the deposition hole, the water retention properties of the rock, and the transmissivity of two fractures intersecting the deposition hole have been varied.

The calculations indicate that the wetting takes about 5 years if the water pressure in the rock is high and if the permeability of the rock is so high that the properties of the bentonite determine the wetting rate. However, it may take considerably more than 30 years if the rock is very tight and the water pressure in the rock is low.

The calculations also show that the influence of the rock structure is rather large except for the influence of the transmissivity T of the fractures, which turned out to be insignificant for the values used in the calculations.

Sammanfattning

Bevätningsprocessen i deponeringshål utförda enligt KBS3-konceptet har modellerats med preliminära finita element beräkningar av den termo-hydro-mekaniska funktionen hos buffert, återfyllning och omgivande berg.. Bufferten har modellerats enligt framtagna preliminära materialmodeller för svällande lera.

Bergets egenskaper har varierats för att undersöka inverkan av bergegenskaper och vattentryck på bevätningsprocessen. De egenskaper som varierats vid modelleringen av deponeringshålen är bergmatrisens permeabilitet, återfyllningens vattentillgång, vattentrycket i det omgivande berget, permeabiliteten hos en störd zon runt deponeringshålet, bergets vattenhållande förmåga och transmissiviteten hos två sprickor som står i kontakt med deponeringshålet..

Beräkningarna indikerar att bevätningen tar cirka 5 år om bergets permeabilitet är så hög att bentoniten egenskaper bestämmer bevätningshastigheten och vattentrycket i berget är högt, men kan ta betydligt längre tid än 30 år om berget är tätt och vattentrycket lågt.

Beräkningarna visar också att inverkan av bergstrukturen är ganska stor med undantag för transmissiviteten hos de två sprickor som simulerats, vars inverkan visade sig vara obefintlig för de värden som användes.

Executive Summary

The wetting process in deposition holes designed according to the KBS3 concept has been modelled with preliminary finite element calculations of the thermo-hydro-mechanical behaviour of the buffer, backfill and surrounding rock. The buffer and backfill materials have been modelled according to the preliminary material models developed for these materials. The properties of the rock have been varied in order to investigate the influence of the rock properties and the hydraulic conditions on the wetting processes.

In the modelling of the **deposition holes** the permeability of the rock matrix, the water supply from the backfill, the water pressure in the surrounding rock, the permeability of the disturbed zone around the deposition hole, the water retention properties of the rock, and the transmissivity of two fractures intersecting the deposition hole have been varied.

These calculations indicate that the wetting takes about 5 years if the water pressure in the rock is high and if the permeability of the rock is so high that the properties of the bentonite determine the wetting rate. However, it may take considerably more than 30 years if the rock is very tight and the water pressure in the rock is low. The calculations also show that the influence of the rock structure is rather large except for the influence of the transmissivity T of the fractures, which turned out to be insignificant for the values used in the calculations.

The results of the calculations show that the influence of most changes in rock properties and boundary conditions are rather large. There is a lack in knowledge of rock properties and interaction buffer/rock and a need for improved material models of the buffer but the calculations yielded the following results concerning the influence of the rock:

A highly permeable rock with $K = 10^{-10}$ m/s yielded that the buffer between the canister and the periphery of the hole was highly saturated within a few years and it took up to 10 years to get complete saturation in the entire buffer if the water pressure in the surrounding rock was low. These results are expected to be typical when the hydraulic conductivity is much higher in the rock than in the buffer. When the rock is less or equally permeable as the buffer the wetting is delayed by the flow resistance of the rock.

When water pressure corresponding to hydrostatic at the depth 500 m was present in a boundary 10 m from the deposition hole the rate of wetting was increased considerably (20%-60% reduction in time to saturation), especially at the end of the wetting process.

When there was a 1 cm thick damaged zone with a hydraulic conductivity that is 100 times higher than the rock matrix at the surface of the deposition hole, the time until saturation was reduced up to 35%. The strongest effect was reached when the rock was allowed to de-saturate.

De-saturation in the rock may be important for the saturation rate in the buffer if the rock matrix has a low hydraulic conductivity and if there is a low external water

pressure in the rock. The results showed that influence was strongest for the time to 95% saturation at the radial canister periphery where up to 86% extension of the saturation period was reached. The influence was smaller when a few fractures supplied the buffer with water in combination with a high external water pressure.

Two horizontal fractures that intersected a deposition hole in the described configuration increased the rate of saturation, although the influence was rather limited due to the long distance between the fractures. If the rock was de-saturated the effect was stronger. The influence of fractures was especially strong at the radial periphery of the canister with a decrease in time to 95% saturation of up to 28% when there was a disturbed zone

When the transmissivity of the fractures was changed from 10^{-9} to 10^{-11} m^2/s, which corresponds to an inflow of 4.4 and 0.044 l/h into the empty hole, no change in wetting rate could be observed. The buffer can obviously not utilise the water supplied by large fractures.

No study of the influence of changes in bentonite properties and models has been made. The THM-models are very complicated and neither the models nor the parameters have been sufficiently validated.

Contents

1 Introduction

In the KBS3 concept for storage of nuclear high-level waste in crystalline rock canisters with waste will be deposited in 8 m deep holes with the diameter 1.75 m at 500 m depth. The canisters will be surrounded by highly compacted swelling clay with low permeability (bentonite) and the tunnels will be backfilled with a mixture of bentonite and crushed rock.

In Äspö Hard Rock Laboratory the KBS3 concept will be tested in an experiment called the Prototype Repository. In this experiment a number of deposition holes and the deposition tunnel will be simulated in full scale. Fig 1-1 shows the layout of the experiment /1-1/.

The buffer and backfill are not saturated with water during installation. Instead about 25% of the total amount of water in the buffer and about 60% in the backfill must be provided by the rock. The water saturation process of both the buffer and the backfill has been studied in a number of finite element calculations where the rock properties, rock structure and water pressure have been varied.

The calculations are coupled thermo-hydro-mechanical. The purpose has been to study the time until completed water saturation and the influence of the rock properties and the water pressure on the saturation process.

Some simplifications have been made in order to make it possible to carry through the calculations. The main one is to simplify the mechanical calculation by assuming that the initial dry density is the same in the entire buffer, which means that the time for completion of the homogenisation is not considered. Another one, which is needed in order to start with the correct amount of water in the buffer, is to distribute the excess water that can be filled into the slot between the blocks and the rock to the distance 10 cm from the rock instead of the actual 5 cm.

Other simplifications are to make both the tunnel and the deposition hole axially symmetric. The fractures that intersect the deposition are horizontal and the fractures that intersect the tunnel are vertical.

The modelling of the buffer in the deposition holes have been separated from the modelling of the backfill in the tunnel. The modelling of the buffer has originally been made as a general study of the water saturation process in a KBS3 repository and is also reported in a separate report /1-2/, but has been adapted to the conditions in Äspö and included in this report.

2 Modelling of THM processes in buffer material with the FEM-code ABAQUS

2.1 General

The finite element code ABAQUS was used for the calculations. ABAQUS is originally designed for non-linear stress analyses. It has been extended very much in the last 5-10 years and today contains a capability of modelling a large range of processes in many different materials as well as complicated three-dimensional geometry.

The code includes special material models for rock and soil and ability to model geological formations with infinite boundaries and in situ stresses by e.g. the own weight of the medium. Detailed information of the available models, application of the code and the theoretical background is given in the ABAQUS Manuals /2-1/.

The model of water-unsaturated swelling clay described in this chapter and used in these calculations is preliminary and especially the mechanical and vapour flux parts need to be improved.

2.2 Hydro-mechanical analyses in ABAQUS

The hydro-mechanical model consists of porous medium and wetting fluid and is based on equilibrium, constitutive equations, energy balance and mass conservation using the effective stress theory.

Equilibrium

Equilibrium is expressed by writing the principle of virtual work for the volume under consideration in its current configuration at time t:

$$\int_V \sigma : \delta\varepsilon \, dV = \int_S \mathbf{t} \cdot \delta\mathbf{v} \, dS + \int_V \hat{\mathbf{f}} \cdot \delta\mathbf{v} \, dV, \tag{2-1}$$

where $\delta\mathbf{v}$ is a virtual velocity field, $\delta\varepsilon \stackrel{def}{=} sym(\partial\delta\mathbf{v}/\partial\mathbf{x})$ is the virtual rate of deformation, σ is the true (Cauchy) stress, $\mathbf{t}$ are the surface tractions per unit area, and $\hat{\mathbf{f}}$ are body forces per unit volume. For our system, $\hat{\mathbf{f}}$ will often include the weight of the wetting liquid,

$$\mathbf{f}_w = S_r n \rho_w \mathbf{g}, \tag{2-2}$$

where S_r is the degree of saturation, n the porosity, ρ_w the density of the wetting liquid and **g** is the gravitational acceleration, which we assume to be constant and in a constant direction (so that, for example, the formulation cannot be applied directly to a centrifuge experiment unless the model in the machine is small enough that g can be treated as constant). For simplicity we consider this loading explicitly so that any other gravitational term in $\hat{\mathbf{f}}$ is only associated with the weight of the dry porous medium. Thus, we write the virtual work equation as

$$\int_V \sigma : \delta \varepsilon \, dV = \int_S \mathbf{t} \cdot \delta \mathbf{v} \, dS + \int_V \mathbf{f} \cdot \delta \mathbf{v} \, dV + \int_V S_r n \rho_w \mathbf{g} \cdot \delta \mathbf{v} \, dV, \tag{2-3}$$

where **f** are all body forces except the weight of the wetting liquid.

The simplified equation used in ABAQUS for the effective stress is:

$$\bar{\sigma}^* = \sigma + \chi \, u_w \mathbf{I}. \tag{2-4}$$

where σ is the total stress, u_w is the pore water pressure, χ is a function of the degree of saturation (usual assumption $\chi = S_r$), and **I** the unitary matrix.

Energy balance

The conservation of energy implied by the first law of thermodynamics states that the time rate of change of kinetic energy and internal energy for a fixed body of material is equal to the sum of the rate of work done by the surface and body forces. This can be expressed as:

$$\frac{d}{dt} \int_V \left(\tfrac{1}{2} \rho \mathbf{v} \cdot \mathbf{v} + \rho U \right) dV = \int_S \mathbf{v} \cdot \mathbf{t} \, dS = \int_V \mathbf{f} \cdot \mathbf{v} \, dV, \tag{2-5}$$

where

ρ is the current density,

v is the velocity field vector,

U is the internal energy per unit mass,

t is the surface traction vector,

f is the body force vector, and

Constitutive equations

The constitutive equation for the solid is expressed as:

$$d\tau^c = \mathbf{H} : d\varepsilon + \mathbf{g},$$ (2-6)

where $d\tau^c$ is the stress increment, $\mathbf{H}$ the material stiffness, $d\varepsilon$ the strain increment and $\mathbf{g}$ is any strain independent contribution (e.g. thermal expansion). $\mathbf{H}$ and $\mathbf{g}$ are defined in terms of the current state, direction for straining, etc., and of the kinematic assumptions used to form the generalised strains.

The constitutive equation for the liquid (static) in the porous medium is expressed as:

$$\frac{\rho_w}{\rho_w^0} \approx 1 + \frac{u_w}{K_w} - \varepsilon_w^{th},$$ (2-7)

where ρ_w is the density of the liquid, ρ_w^0 is its density in the reference configuration, $K_w(T)$ is the liquid's bulk modulus, and

$$\varepsilon_w^{th} = 3\alpha_w (T - T_w^0) - 3\alpha_{w|T^I} (T^I - T_w^0)$$ (2-8)

is the volumetric expansion of the liquid caused by temperature change. Here $\alpha_w(T)$ is the liquid's thermal expansion coefficient, T is the current temperature, T^I is the initial temperature at this point in the medium, and T_w^0 is the reference temperature for the thermal expansion. Both u_w/K_w and ε_w^{th} are assumed to be small.

Mass conservation

The mass continuity equation for the fluid combined with the divergence theorem implies the pointwise equation:

$$\frac{1}{J}\frac{d}{dt}(J\rho_w S_r n) + \frac{\partial}{\partial \mathbf{x}} \cdot (\rho_w S_r n \mathbf{v}_w) = 0.$$ (2-9)

where J is the determinant of the Jacobian matrix and $\mathbf{x}$ is position. The constitutive behaviour for pore fluid is governed by Darcy's law, which is generally applicable to low fluid velocities. Darcy's law states that, under uniform conditions, the volumetric flow rate of the wetting liquid through a unit area of the medium, $S_r n \mathbf{v}_w$, is proportional to the negative of the gradient of the piezometric head:

$$S_r n \mathbf{v}_w = -\hat{\mathbf{k}} \frac{\partial \phi}{\partial \mathbf{x}},$$ (2-10)

where $\boxed{\times}$ is the permeability of the medium and ϕ is the piezometric head, defined as:

$$\phi \overset{def}{=} z + \frac{u_w}{g\rho_w}$$ (2-11)

where z is the elevation above some datum and g is the magnitude of the gravitational acceleration, which acts in the direction opposite to z. $\hat{k}$ can be anisotropic and is a function of the saturation and void ratio of the material. $\hat{k}$ has units of velocity (length/time). [Some authors refer to $\hat{k}$ as the hydraulic conductivity and define the permeability as

$$\hat{K} = \frac{v}{g}\hat{k}$$ (2-12)

where v is the kinematic viscosity of the fluid.]

We assume that g is constant in magnitude and direction, so

$$\frac{\partial \phi}{\partial x} = \frac{1}{g\rho_w}\left(\frac{\partial u_w}{\partial x} - \rho_w g\right)$$ (2-13)

Vapour flow

Vapour flow is modelled as a diffusion process driven by a temperature gradient (coded as UEL user supplied routine with stiffness and flow).

$$\mathbf{q}_v = -D_{Tv}\frac{\partial T}{\partial x}$$ (2-14)

where $\mathbf{q}_v$ is the vapour flux and D_{Tv} the thermal vapour diffusivity.

2.3   Uncoupled heat transfer analysis

Energy balance

The basic energy balance is

$$\int_V \rho \dot{U}dV = \int_S q dS + \int_V r dV$$ (2-15)

where V is a volume of solid material, with surface area S; ρ is the density of the material; $\dot{U}$ is the material time rate of the internal energy; q is the heat flux per unit area of the body, flowing into the body; and r is the heat supplied externally into the body per unit volume.

It is assumed that the thermal and mechanical problems are uncoupled in the sense that $U = U(T)$ only, where T is the temperature of the material, and q and r do not depend on

the strains or displacements of the body. For simplicity a Lagrangian description is assumed, so "volume" and "surface" mean the volume and surface in the reference configuration.

Constitutive definition

The relationship is usually written in terms of a specific heat, neglecting coupling between mechanical and thermal problems:

$$\boxed{\times}$$

(2-16)

Heat conduction is assumed to be governed by the Fourier law.

$$\mathbf{f} = -\mathbf{k}\frac{\partial T}{\partial \mathbf{x}}$$

(2-17)

where $\mathbf{f}$ is the heat flux and $\mathbf{k}$ is the heat conductivity matrix, $\mathbf{k} = \mathbf{k}(T)$. The conductivity can be fully anisotropic, orthotropic, or isotropic.

2.4 Coupling of thermal and hydro-mechanical solutions

In ABAQUS the coupled problem is solved through a "staggered solution technique" as sketched in Fig 2-1 and below.

1. First a thermal analysis is performed where heat conductivity and specific heat are defined as functions of saturation and water content. In the first analysis these parameters are assumed to be constant and in the subsequent analyses they are read from an external file.

2. The hydromechanical model calculates stresses, pore pressures, void ratios, degree of saturation etc. as function of time. Saturation and void ratio histories are written onto an external file.

3. The material parameters update module reads the file with saturation and void ratio data and creates a new file containing histories for saturation and water content. The saturation and water content histories are used by the thermal model in the following analysis.

4. Steps 1-3 are repeated if parameter values are found to be different compared to those of the previous solution.
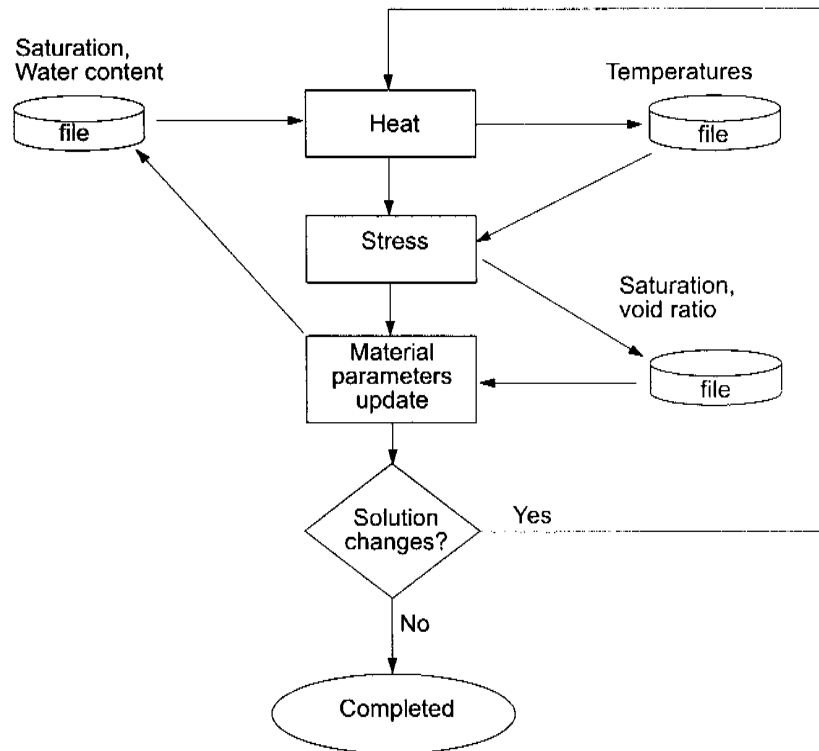
Figure 2-1. In ABAQUS, heat transfer calculations and hydro-mechanical calculations are decoupled. By using the iteration procedure schematically shown above, the effects of a fully coupled THM model are achieved.

3 Description of the parameters in the material model of the buffer

3.1 Processes

3.1.1 Thermal flux from conduction

The only thermal flux that is modelled is thermal conduction with the following parameters:

λ = thermal conductivity

c = specific heat

3.1.2 Water liquid flux

The water flux in the liquid phase is modelled to be governed by Darcy's law with the water pressure difference as driving force in the same way as for water saturated clay.

The magnitude of the hydraulic conductivity K_p of partly saturated clay is a function of the void ratio, the degree of saturation and the temperature. K_p is assumed to be a function of the hydraulic conductivity K of saturated clay and the degree of saturation S_r according to Eqn 3-1.

$$K_p = (S_r)^\delta K \tag{3-1}$$

where

K_p = hydraulic conductivity of partly saturated soil (m/s)

K = hydraulic conductivity of completely saturated soil (m/s)

δ = parameter (usually between 3 and 10)

Water transport driven by gravity and density gradients is included in the model as well.

3.1.3 Water vapour flux

The water vapour flux is modelled as a diffusion processes driven by the temperature gradient and the water vapour pressure gradient (at isothermal conditions) according to Eqn 3-2:

$$q_v = -D_{Tv}\nabla T - D_{pv}\nabla p_v \tag{3-2}$$

where

q_v = vapour flow

D_{Tv} = thermal vapour flow diffusivity

T = temperature

D_{pv} = isothermal vapour flow diffusivity

p_v = vapour pressure

The isothermal vapour flow is neglected and thus $D_{pv} = 0$.

The thermal water vapour diffusivity D_{Tv} can be evaluated from moisture redistribution tests by calibration calculations. The following relations were found to yield acceptable results /3-1/:

$$D_{Tv} = D_{Tvb} \qquad\qquad 0.3 \leq S_r \leq 0.7 \tag{3-3}$$

$$D_{Tv} = D_{Tvb} \cdot cos^a\left(\frac{S_r - 0.7}{0.3} \cdot \frac{\pi}{2}\right) \quad S_r \geq 0.7 \tag{3-4}$$

$$D_{Tv} = D_{Tvb} \cdot sin^b\left(\frac{S_r}{0.3} \cdot \frac{\pi}{2}\right) \qquad S_r \leq 0.3 \tag{3-5}$$

a and b are factors that regulates the decreased vapour flux at high and low degree of saturation.

The diffusivity is thus constant with a basic value D_{Tvb} between 30% and 70% degree of saturation. It decreases strongly to $D_{Tv} = 0$ at 0% and 100% saturation. The influence of temperature and void ratio on the diffusivity is not known and not considered in the model.

3.1.4 Hydraulic coupling between the pore water and the pore gas

The pore pressure u_w of the unsaturated buffer material, which is always negative, is modelled as being a function of the degree of saturation S_r independent of the void ratio.

$$u_w = f(S_r)$$ (3-6)

ABAQUS also allows for hysteresis effects, which means that two curves may be given (drying and wetting curves)

The pore air pressure is not modelled.

3.1.5 Mechanical behaviour of the structure

The mechanical behaviour has been modelled with a non-linear Porous Elastic Model and Drucker-Prager Plasticity model. The effective stress theory is applied and adapted to unsaturated conditions according to Eqn 2-4 by Bishop. The shortcoming of the effective stress theory is compensated for by a correction called moisture swelling (see chapter 3.1.8).

The *Porous Elastic Model* implies a logarithmic relation between the void ratio e and the average effective stress p according to Eqn 3-7.

$$\Delta e = \kappa \Delta \ln p$$ (3-7)

where $\kappa =$ porous bulk modulus

Poisson's ratio v is also required.

Drucker Prager Plasticity model contains the following parameters:

β = friction angle in the p-q plane

d = cohesion in the p-q plane

ψ = dilation angle

q $= f(\varepsilon^d_{pl}) =$ yield function

The yield function is the relation between Mises' stress q and the plastic deviatoric strain ε^d_p at a specified stress path. The dilation angle determines the volume change during shear.

3.1.6 Thermal expansion

The volume change caused by the thermal expansion of water and particles can be modelled with the parameters

$\alpha_s =$ coefficient of thermal expansion of solids (assumed to be 0)

$\alpha_w =$ coefficient of thermal expansion of water

Only the expansion of the separate phases is taken into account. The possible change in volume of the structure by thermal expansion (not caused by expansion of the separate phases) is not modelled. However, a thermal expansion in water volume will change the degree of saturation which in turn will change the volume of the structure.

3.1.7 Mechanical behaviour of the separate phases

The water and the particles are mechanically modelled as separate phases with linear elastic behaviour. The pore air is not mechanically modelled.

3.1.8 Mechanical coupling between the structure and the pore water

<u>Effective stress theory</u>

The effective stress concept according to Bishop is used for modelling the mechanical behaviour of the water-unsaturated buffer material:

$$s_e = (s - u_a) + \chi(u_a - u_w) \tag{3-8}$$

Eqn 3-8 is simplified in the following way:

$u_a = 0$ (no account is taken to the pressure of enclosed air)

$$\chi = S_r$$

<u>Moisture swelling</u>

The shortcomings of the effective stress theory can be partly compensated in ABAQUS by a correction called "moisture swelling". This procedure changes the volumetric strain ε_v by adding a strain that can be made a function of the degree of saturation S_r:

$$\Delta\varepsilon_v = f(S_r) \tag{3-9}$$

3.2 Required parameters

The required input parameters for the described THM model (ABAQUS) are the following:

Thermal

- Tables of thermal conductivity λ and specific heat c as function of void ratio e and degree of saturation S_r.

Hydraulic

- Table of the hydraulic conductivity of water saturated material K as function of void ratio e and temperature T.

- Influence of degree of saturation S_r on the hydraulic conductivity K_p expressed as the factor δ in Eqn 3-1.

- The basic water vapour flow diffusivity D_{vTb} and the parameters a and b in Eqns 3-3 to 3-5.

- Table of the matric suction u_w as a function of the degree of saturation S_r.

Mechanical

- Porous bulk modulus κ according to Eqn 3-7 and Poisson's ratio ν.

- Drucker Prager plasticity parameters β, d, ψ, and the **yield function**.

- Bulk modulus and coefficient of thermal expansion of water (B_w, α_w)and bulk modulus solids (B_s).

- Bishops parameter χ in Eqn 3-8 (usual assumption $\chi = S_r$).

- The volume change correction ε_v as a function of the degree of saturation S_r (the "moisture swelling" procedure).

Initial conditions

The following initial conditions of the elements in the structure need to be specified:

- void ratio e

- degree of saturation S_r

- pore pressure u

- average effective stress p

3.3 Calibration tests

Most of the required parameters can be determined with direct measurements in the laboratory. However, the following parameters cannot be directly measured:

δ, D_{vTb}, a, b, χ and the "moisture swelling" procedure.

These parameters need to be calibrated with some indirect tests. It can be done with the following sequence of calibration tests:

Drying and wetting tests

Unconfined samples at the initial void ratio and degree of saturation are dried or wetted by changing the relative humidity in the surrounding air. After equilibrium the density and water ratio of each sample are measured and the relation between the void ratio and the degree of saturation is determined.

The drying and wetting tests are then simulated with the code and the measured and calculated results compared. Since the effective stress theory is not valid the curves will not coincide. The difference is used to determine χ and the "moisture swelling" data. Usually $\chi = S_r$ is assumed and the difference in volume change directly calculated and used for the "moisture swelling" procedure.

Swelling pressure tests

The swelling pressure measured at the initial void ratio after completed saturation is used to check that the applied "moisture swelling" procedure yields the correct swelling pressure by simulating a swelling pressure test. If the calculated swelling pressure disagrees with the measured one, the "moisture swelling" procedure must be changed. A conflict may appear which has to be solved either by making a compromise and accept some difference or by applying another relation for χ.

Water uptake tests

When the mechanical parameters have been determined the influence of the degree of saturation on the hydraulic conductivity can be checked. The factor δ in Eqn 5-1 can be determined with a number of water uptake tests. These tests are made by confining samples with a low degree of saturation in stiff cylinders and apply a filter stone with zero water pressure at one end. The negative water pressure of the unsaturated sample will suck water into the sample. After a certain time, which must be different for all samples, the test is brought to an end. The sample is then sliced into a number of pieces and the water ratio (and if possible also the density) of each piece determined.

With these tests the degree of saturation (and void ratio) can be plotted as a function of the distance from the water inlet. By simulating the same test with the code the factor δ in Eqn 3-1 can be calibrated.

Temperature gradient tests

Finally, the thermal vapour flow diffusivity can be determined with a number of temperature gradient tests. These tests can be performed in a stiff oedometer with water

tight boundaries by applying a constant temperature gradient along the sample. The tests are finished after different times and the sample sliced in the same way as in the previous tests.

With these tests the degree of saturation (and void ratio) can be plotted as a function of the distance to the hot end. By simulating the test with the code D_{vTb}, a, and b in Eqns 5-3 to 5-5 can be calibrated.

Calibration sequence

The calibration of the different parameters must be made in the mentioned sequence, since the parameters δ, D_{vTb}, a, and b are not required for simulating the first two tests and D_{vTb}, a, and b are not required for simulating the water uptake test, while all parameters are required for the temperature gradient test.

4 Element mesh and boundary condition

The element mesh is shown in Fig 4-1. The elements are 2D axial symmetric with the symmetry axis in the centre of the deposition hole. The backfill material, the buffer material, the canister, the rock matrix, and the damaged zone of the rock around the deposition hole are modelled. In some calculations two fractures are included in the model. They are horizontal. One of them intersects the deposition hole in the middle of the canister. The other fracture intersects the deposition hole at the bottom.

The damaged zone has the thickness 1 cm. The fractures are modelled as porous material with the thickness 1 cm.

The mesh is 24 m high and has the radius 11 m. The number of elements is about 2600.

The boundaries of the rock and backfill are **mechanically** fixed, except for in the symmetry axis were the rock, buffer, canister and backfill are mechanically locked in the radial direction but free in the axial direction.

The **thermal** outer boundary has constant temperature of 10 °C and a thermal film coefficient f (heat transfer coefficient) that has been chosen to yield a similar temperature progress in the canister as calculated for a full size repository.

$f = 0.015$ W/m, K

The **hydraulic** outer boundary is fixed either at the water pressure 0 kPa or 5000 kPa.

5 Parameter values for the material model of MX-80

5.1 Reference material

The reference material is Volclay sodium bentonite MX-80. Results from laboratory tests on this material are described by Börgesson et al /5-1; 5-2; 3-2/. The material model presented is preliminary. The initial conditions vary a little between the laboratory tests, but the following values correspond regarding density to the planned average dry density in a KBS3 deposition hole and regarding water content to the planned water ratio in the bentonite blocks after compaction.

- dry density: $\rho_d = 1.67$ g/cm^3 and

- water ratio: $w = 0.17$

which yield

- void ratio: $e = 0.77$ and

- degree of saturation: $S_r = 0.61$.

The water ratio at water saturation is for this void ratio $w = 0.277$.

5.2 Thermal properties

The *thermal conductivity* has been measured as a function of the degree of saturation /5-2/. The results at the void ratio 0.8 are shown in Fig 5-1. The parameter values for the ABAQUS model are shown in Table 5-1 (linear interpolation between the values).

Table 5-1. Thermal conductivity λ of the buffer material as a function of the degree of saturation S_r

S_r	λ W/m,K
0	0.3
0.2	0.3
0.3	0.4
0.4	0.55
0.5	0.75
0.6	0.95
0.7	1.1
0.8	1.2
0.9	1.25
1.0	1.3

The *specific heat* has been calculated as the weight average of the specific heat of water and particles according to Eqn 5-1.

$$c=800/(1+w)+4200w/(1+w) \qquad (5\text{-}1)$$

Eqn 5-1 yields the input parameters shown in Table 5-2 (linear interpolation)

Table 5-2. Heat capacity c of the buffer material as a function of the water ratio w

w	c Ws/m,kg
0	800
0.1	1109
0.2	1367
0.3	1585
1.0	2500

5.3 Hydraulic properties

The *hydraulic conductivity* has been measured at different temperatures and void ratios /5-1/. Some results are shown in Fig 5-2. Table 5-3 shows the values in the model.

Table 5-3. Hydraulic conductivity K as a function of void ratio e and temperature T

T	e	K
°C		m/s
20	0.4	$0.035 \cdot 10^{-13}$
20	0.6	$0.2 \cdot 10^{-13}$
20	0.8	$0.65 \cdot 10^{-13}$
20	1.0	$1.75 \cdot 10^{-13}$
40	0.4	$0.05 \cdot 10^{-13}$
40	0.6	$0.31 \cdot 10^{-13}$
40	0.8	$1.0 \cdot 10^{-13}$
40	1.0	$2.75 \cdot 10^{-13}$
60	0.4	$0.07 \cdot 10^{-13}$
60	0.6	$0.44 \cdot 10^{-13}$
60	0.8	$1.45 \cdot 10^{-13}$
60	1.0	$3.85 \cdot 10^{-13}$
80	0.4	$0.1 \cdot 10^{-13}$
80	0.6	$0.55 \cdot 10^{-13}$
80	0.8	$1.8 \cdot 10^{-13}$
80	1.0	$4.9 \cdot 10^{-13}$

The influence of the degree of saturation is goverened by the parameter δ in Eqn 3-1. For the reference material the standardard value

$$\delta = 3$$

has been found to be satisfactory according to the calibration and validation calculations.

The *thermal vapour flow diffusivity* D_{Tvb} and the parameters a and b according to Eqns 3-2 to 3-4 have been determined with the calibration calculations of the moisture redistribution tests. The following values were chosen:

$$D_{Tvb} = 0.7 \cdot 10^{-11} \ m^2/s,K$$

$$a = 6$$

$$b = 6$$

The *water retention curve* has been determined from measurements of the total suction, the matric suction and the swelling pressure. The measurements have been converted to degree of saturation for the reference density. Fig 5-3 shows the relation used in the model. The retention curve of the rock is also shown.

5.4 Mechanical properties

The following data has been used for the *Porous Elastic* model:

$\kappa = 0.20$

$\nu = 0.4$

The value of κ has been derived from oedometer and swelling pressure tests /5-1/. Fig 5-4 shows the measured swelling pressure as a function of void ratio.

The following data was used for the *Drucker Prager Plasticity* model

$\beta = 16°$

$d = 100$ kPa

$\psi = 2°$

Table 5-5. Yield function

q (kPa)	ε_{pl}
1	0
50	0.005
100	0.02
150	0.04
200	0.1

The friction angle in the q-p plane and the dilation angle were taken from triaxial test results shown in Fig 5-5 /5-1/ with the curved failure line approximated to a straight line.

The following standard values has been used for the *properties of the water and solid phases*:

$B_w = 2.1 \cdot 10^6$ kPa (bulk modulus of water)

$B_s = 2.1 \cdot 10^8$ kPa (bulk modulus of solids)

$\alpha_w = 3.0 \cdot 10^{-4}$ (coefficient of thermal volumetric expansion of water)

$\alpha_s = 0$ (coefficient of thermal expansion of solids)

$\rho_w = 1000$ kg/m^3 (density of water)

$\rho_s = 2780$ kg/m^3 (density of solids)

The parameters used for calculating the *effective stress* are χ in Eqn 3-6 and the moisture swelling data:

$$\chi = S_r$$

The data for the *moisture swelling* procedure is taken from calibration tests and includes a long list of volumetric strain corrections $\Delta\varepsilon_v$. Table 5-6 shows a selection of values from this table.

Table 5-6. Change in volumetric strain ε_v as a function of the degree of saturation S_r used in the "moisture swelling" procedure (selection of curtailed data)

S_r	$\Delta\varepsilon_v$
0	-0.2
0.1	-0.01
0.2	0.02
0.3	0.03
0.4	0.02
0.5	0.01
0.6	0
0.7	-0.02
0.8	-0.03
0.88	-0.04
0.94	-0.06
0.97	-0.11
0.99	-0.24
1.0	-0.81

5.5 Calibration and validation calculations for MX-80

5.5.1 General

As mentioned earlier some of the parameters have been determined or validated indirectly by calibration with laboratory tests. The laboratory tests are described by Börgesson et al /3-1/. This chapter shows some of these calculations. The derived parameter values are preliminary since the measured results in some tests are derived from tests on material with different initial conditions. Only the final calculations with the chosen parameters will be shown.

5.5.2 Drying and wetting tests

An example of a drying test is shown in Fig 5-6. The void ratio is plotted as a function of the water ratio. Such a test has been simulated by starting with the reference properties $e=0.77$ and $w=0.17$ and using the material model without the moisture swelling procedure. Since the measurement did not start at the reference properties an imaginary test, that has been assumed to have the same $e\text{-}w$ inclination, has been used for the calibration. The difference in results between the calculated and the "measured" relation was then used as input data for the moisture swelling procedure.

5.5.3 Swelling pressure tests

Two kinds of calculations of the swelling pressure have been done. One swelling pressure test was simulated by running the drying wetting test from the reference properties ($e=0.77$, $S_r=0.61$) to complete saturation under constant volume, which yields that a swelling pressure is received instead of a swelling. The simulation and comparison yield:

- Calculated swelling pressure: 8.1 MPa

- Measured swelling pressure (according to Fig 5-4): 6-8 MPa.

In the other calculation a swelling pressure test with water applied at one end of a 5 cm thick sample inside a stiff oedometer was simulated. The same element mesh and calculation technique was used as for the water uptake tests, which will be described in chapter 5.6. The initial condition differed from the reference case. $e=0.75$ and $S_r=0.4$ were applied as initial conditions:

The calculated swelling pressure is shown in Fig 5-7 as a function of time.

- Calculated swelling pressure: 9.6 MPa

- Measured swelling pressure (Fig 5-4): 7-10 MPa

The calculated final swelling pressure 9.6 MPa is reached after about $5 \cdot 10^6$ s which correspond to about 2 months.

5.6 Water uptake tests

Water uptake tests have been made at different densities and initial water ratios /3-1/. In these tests water was applied at one end of a 50 mm high sample confined in a stiff oedometer and the axial water ratio distribution measured at different times after start.

The calculations were made with the initial conditions $e=0.75$ and $S_r=0.4$. The sample was supplied with water by applying the water pressure 0 kPa in the bottom boundary.

The calculated degree of saturation as a function of the distance from the water inlet at three times is shown in Fig 5-8 together with the measured values at corresponding times The agreement is rather good.

5.7 Temperature gradient tests

Several temperature gradient tests at different water ratios and temperatures have been performed /3-1/. Unfortunately these tests were made at the void ratio 1.0 which differs from the reference case. The calibration must thus be considered to be preliminary and new tests need to be performed. The tests were done with a temperature gradient applied along a 5 cm long sample, which was both mechanically and hydraulically confined. The water ratio distribution was measured at different times.

The calculation was done with a 2D element mesh with 20 equally large elements simulating the 5 cm high sample. The model has hydraulically and mechanically confined boundaries. The reference parameter values were used for this calculation (e=0.77, S_r=0.61).

Several calculations of this test were done with different values of the water vapour diffusivity until the agreement between measured and calculated degree of saturation were acceptable (D_{Tvb}=0.7·10^{-11} m^2/s,K).

Fig 5-9 shows the measured and calculated degree of saturation as a function of the distance from the cold end at different times.

5.8 Initial conditions

The mechanical processes at the swelling and homogenisation of the block and the 5 cm slot filled with pellets are not simulated. Instead the average void ratio of the buffer is used for the entire buffer. However, the inhomogeneous water ratio distribution is simulated by distributing the surplus water in the 5 cm wide slot over a 10 cm wide zone in the periphery. By starting with a 10 cm zone that is water saturated, the right total amount of water is used. The reason for neglecting the homogenisation process is that the large change in density that will take place makes the applied retention curve incorrect. Thus the buffer is divided into two materials with the same void ratio but different initial degree of saturation:

Buffer 1

A 10 cm thick zone in the periphery of the deposition hole with the following initial conditions:

e = 0.77 (void ratio)

S_r = 1.0 (degree of saturation)

which yields

$w = 0.277$ (water ratio)

$\rho_d = 1.57$ (dry density)

$\rho_m = 2.01$ (density at saturation)

Two more initial conditions are required:

$u = 0$ kPa (pore pressure)

$p = 0$ kPa (average effective stress)

Buffer 2

The rest of the buffer with the following initial conditions:

$e = 0.77$ (void ratio)

$S_r = 0.61$ (degree of saturation)

which yields

$w = 0.169$ (water ratio)

$\rho_d = 1.57$ (dry density)

$\rho_m = 2.01$ (density at saturation)

Two more initial conditions are required:

$u = -31\ 000$ kPa (pore pressure)

$p = 18\ 910$ kPa (average effective stress)

which yields

$p_{tot} = 0$ kPa (total pressure)

6 Material properties of other materials

6.1 General

All other materials are mechanically modelled as linear elastic, hydraulically modelled as porous media, and thermally modelled with heat conduction.

6.2 Backfill

The material model of the backfill is simplified since the behaviour is not of primary interest in other respect than that it must interact with the buffer material in a relevant way. Hydraulically it is modelled to be water saturated from start with a porous behaviour governed by Darcy's law. The following parameter values were used:

$E = 30$ MPa

$v = 0.3$

$\rho = 2000$ kg/m^3 (bulk density)

$K = 2 \cdot 10^{-10}$ m/s or $1 \cdot 10^{-14}$ m/s

$\lambda = 1.5$ W/m,K

$c = 1200$ Ws/kg,K

6.3 Rock

6.3.1 General

The rock matrix, the disturbed zone around the deposition hole and the fractures were modelled with different properties. The mechanical and thermal properties were assumed to be the same since those processes were not studied in detail. The following parameter values were used for all rock parts:

$E = 1850$ MPa

$v = 0.3$

$\rho = 2600 \text{ kg/m}^3$

$\lambda = 3.0 \text{ W/m,K}$

$c = 800 \text{ Ws/kg,K}$

6.3.2 Hydraulic properties

The hydraulic conductivity of the different rock parts were varied within the following ranges:

Rock matrix: $K = 10^{-10}$ m/s - 10^{-14} m/s

EDZ: K = same as the rock matrix or 10^{-11} m/s

Fractures: 1 cm thick with K = same as the rock matrix or 10^{-7} m/s - 10^{-9} m/s

In some calculations the rock has been allowed to de-saturate. The retention curve has not been measured but the values shown in Table 6-1 and Fig 5-3 have been used.

Table 6-1. Retention curve of the rock with the pore pressure u as a function of the degree of saturation S_r

S_r	u (kPa)
0.01	-20 000
0.1	-10 000
0.2	-9 000
0.3	-8 000
0.4	-7 000
0.5	-6 000
0.6	-5 000
0.7	-4 000
0.8	-3 000
0.9	-2 000
0.99	-1 000
1.0	0

The hydraulic conductivity of partly saturated rock K_p is assumed to be a function of the hydraulic conductivity K of saturated rock and the degree of saturation S_r according to Eqn 6-1.

$$K_p = (S_r)^\delta K \tag{6-1}$$

where

$\delta = 3$

6.4 Heater

The heater was modelled as hydraulically impermeable with the following mechanical and thermal properties:

$E = 2.1 \cdot 10^5$ MPa

$v = 0.3$

$\rho = 7000$ kg/m^3

$\lambda = 200$ W/m,K

$c = 400$ Ws/kg,K

7   Calculations

7.1   General

The calculations are divided into thermal and hydro-mechanical calculations. The hydro-mechanical calculation is coupled but the thermal calculation has not been coupled to the hydro-mechanical in order to simplify the calculations. Only one thermal calculation has been done, using the initial values of degree of saturation for the applied thermal conductivity of the buffer material. This simplification overestimates the thermal gradient in the buffer after some time, but the effect on the water saturation process is considered to be small compared to the effect of the difference in hydraulic properties of the rock in the different calculations.

The power generation in the canister has been modelled with the reference initial power 1050 W and a power decay with time according to Eqn 7-1, which has been derived from the power generation in a reference KBS3 canister with the distance 40 m between deposition tunnels /7-1/.

$$P(t) = P_0[c_1 \exp(0.02t) + c_2 \exp(0.002t) + c_3 \exp(0.0002t)] \tag{7-1}$$

where

$P(t)$ = canister power (W)

t = time (years)

P_0 = canister power at deposition = 1680 W

$c_1 = 0.769$

$c_2 = 0.163$

$c_3 = 0.067$

The temperature is strongly influenced by the neighbouring canisters, which are not modelled in this calculation. Instead the thermal boundary conditions have been adapted to yield the maximum canister temperature 75 °C (see chapter 4), which also means that the chosen values of thermal conductivity of the rock is not very important for the temperature results.

7.2   Thermal results

The results of the temperature calculation are shown in Figs 7-1 and 7-2. Fig 7-1 shows the temperature in the buffer at mid height canister as a function of time. Maximum temperature at the canister surface is reached after 19 years. Fig 7-2 shows the temperature distribution after 16 years.

7.3   Hydro-mechanical results

7.3.1   General

16 different hydro-mechanical calculations have been done, with the issue to investigate the hydro-mechanical behaviour during the saturation process and the influence of rock properties on the time until saturation. The following properties and conditions have been varied:

- Hydraulic conductivity of the rock matrix (10^{-10} m/s, 10^{-13} m/s, or 10^{-14} m/s)

- Hydraulic conductivity of the damaged zone around the deposition hole (equal to the rock matrix or 100 times higher)

- Hydraulic conductivity of the two fractures that intersect the deposition hole (equal to the rock matrix, 10^{-7} m/s, 10^{-8} m/s, or 10^{-9} m/s)

- Hydraulic conductivity of the backfill (10^{-14} m/s or $2 \cdot 10^{-10}$ m/s)

- Water pressure at the rock boundary (0 kPa or 5000 kPa)

- De-saturation of rock (the rock can take any negative pore pressure or the rock will de-saturate according to the retention curve)

An overview of the hydro-mechanical calculations is shown in Table 7-1. The table also shows the calculated time until the entire buffer material has a degree of saturation that is higher than 95% and 99%

The results are also shown in history plots (functions of time from start) and contour plots of degree of saturation, pore water pressure and total stress. The degree of saturation can by definition not exceed 100% but some of the contour plots show values higher than 100%, due to extrapolation inaccuracies. The calculations never yield a degree of saturation higher than 100%, but the contour plots are made from extrapolation of integration points inside the elements to nodes at the corners of the elements. The values at the nodes can thus be higher than 100% if one integration point has the degree of saturation 100% and another in the same element has a degree of saturation lower than 100%.

Table 7-1a. Parameter variation of all calculations and time until completed saturation of the buffer material

(1)	(2)	(3)	(4)	(5)	(6)	(7)	(8)	(9)	(10)	(11)
Calc. No	K (rock) m/s	K (EDZ) m/s	$K(T)$ (fract.) m/s (m²/s)	K (backf.) m/s	Water pressure kPa	Unsatu-rated rock	Time to S_r>99% at canister lid years	Time to S_r>95% at canister lid years	Time to S_r>99% at canister periphery years	Time to S_r>95% at canister periphery years
Stress_1	10^{-10}	10^{-10}	10^{-10}	$2 \cdot 10^{-10}$	0	No	10.5	6.7	7.6	2.4
Stress_1b	10^{-10}	10^{-10}	10^{-10}	$2 \cdot 10^{-10}$	5000	No	6.0	5.0	2.9	1.5
Stress_2a	10^{-14}	10^{-14}	10^{-14}	10^{-14}	0	No	>>32	>>32	>>32	>>32
Stress_2b	10^{-14}	10^{-14}	10^{-14}	10^{-14}	5000	No	>>32	>>32	>>32	>>32
Stress_3a	10^{-13}	10^{-13}	10^{-13}	$2 \cdot 10^{-10}$	0	No	24	13.6	20.3	11.1
Stress_3b1	10^{-13}	10^{-13}	10^{-13}	$2 \cdot 10^{-10}$	5000	No	12.4	10.6	11.4	7.5
Stress_3b2	10^{-13}	10^{-11}	10^{-13}	$2 \cdot 10^{-10}$	5000	No	10.8	9.4	10.1	7.3
Stress_3a_o	10^{-13}	10^{-13}	10^{-13}	$2 \cdot 10^{-10}$	0	Yes	~35	20.3	~35	20.6
Stress_3b1_o	10^{-13}	10^{-13}	10^{-13}	$2 \cdot 10^{-10}$	5000	Yes	15.0	12.2	14.4	11.3
Stress_3b2_o	10^{-13}	10^{-11}	10^{-13}	$2 \cdot 10^{-10}$	5000	Yes	11.9	10.1	11.5	8.2

Table 7-1b. Parameter variation of all calculations and time until completed saturation of the buffer material (continuation)

(1)	(2)	(3)	(4)	(5)	(6)	(7)	(8)	(9)	(10)	(11)
Calc. No	K (rock) m/s	K (EDZ) m/s	K (T) (fract.) m/s (m²/s)	K (backf.) m/s	Water pressure kPa	Unsaturated rock	Time to S_r>99% years	Time to S_r>95% at canister lid years	Time to S_r>99% at canister periphery years	Time to S_r>95% at canister periphery years
Stress2_3b1	10^{-13}	10^{-13}	10^{-8} (10^{-10})	$2 \cdot 10^{-10}$	5000	No	10.8	9.5	9.8	7.3
Stress2_3b2	10^{-13}	10^{-11}	10^{-8} (10^{-10})	$2 \cdot 10^{-10}$	5000	No	9.2	8.2	7.6	5.4
Stress2_3b1_o	10^{-13}	10^{-13}	10^{-8} (10^{-10})	$2 \cdot 10^{-10}$	5000	Yes	12.0	10.8	11.2	9.1
Stress2_3b2_o	10^{-13}	10^{-11}	10^{-8} (10^{-10})	$2 \cdot 10^{-10}$	5000	Yes	9.4	8.6	8.2	5.9
Stress2_3b1_oa	10^{-13}	10^{-13}	10^{-7} (10^{-9})	$2 \cdot 10^{-10}$	5000	Yes	12.0	10.8	11.2	9.1
Stress2_3b1_ob	10^{-13}	10^{-13}	10^{-9} (10^{-11})	$2 \cdot 10^{-10}$	5000	Yes	12.0	10.8	11.2	9.1

Column (1) shows the name of the calculation

Column (2) shows the hydraulic conductivity of the rock matrix

Column (3) shows the hydraulic conductivity of the 1 cm wide disturbed zone of the rock around the deposition hole. Bold denotes that the disturbed zone is more permeable than the rock matrix.

Column (4) shows the hydraulic conductivity of the 1 cm wide fractures intersecting the deposition hole. Bold denotes that there is a fracture with increased hydraulic conductivity. For these fractures the corresponding transmissivity T has been given within parenthesis.

Column (5) shows the hydraulic conductivity of the backfill material. Bold denotes that water can go through the backfill, which has a realistic hydraulic conductivity.

Column (6) shows the water pressure at the rock boundary

Column (7) states if the rock has been modelled with ability to become unsaturated

Columns (8) and (9) show the time until the buffer material is 99% and 95% water saturated in the centre of the canister lid on top of the canister. This is usually the last point to be saturated.

Columns (10) and (11) show the time until the buffer material is 99% and 95% water saturated at the radial periphery of the canister, that is when the entire radial bentonite protection is water saturated.

The results will be presented and compared by analysing the influence of the different conditions and parameter variations.

7.3.2 Extreme conditions

In the first four calculations (Stress_1, 1b, 2a, and 2b) the rock conditions are relatively extreme. Stress_1 and 1b have a rock that is so fractured (or has a permeable rock matrix) that the entire rock can be given the hydraulic conductivity 10^{-10} m/s. Stress_2a and 2b have a rock matrix with very low hydraulic conductivity (10^{-14} m/s) and no fractures.

Some results of calculation Stress_1 are shown in Figs 7-3 to 7-6. Figs 7-3 and 7-4 show the distribution of the degree of saturation in the buffer at different times. The entire buffer is more than 95% saturated after 6.7 years. Fig 7-5 has two diagrams. One of them shows the distribution of the degree of saturation along the radial line on the top of the canister at different times. The other one shows the displacement of the canister and the displacement of the centre of the boundary between the buffer and the backfill as a function of time. The canister is displaced about 1 mm upwards while the backfill is lifted 7 cm. Fig 7-6 shows the degree of saturation of equidistant points along the radial

line on the top of the canister. The last point to be saturated is the centre point on top of the canister with a degree of saturation larger than 99 % after $0.32 \cdot 10^9$ s or 10.5 years.

The pore water pressure change in the rock is small during the entire saturation phase. The first year the rock near the deposition hole gets a negative pore water pressure of a few hundred kPa but after one year it is close to 0.

As shown in Table 7-1a and Fig 7-6 the time from 95% to 99% degree of saturation is rather long especially at the radial canister periphery between the canister and the rock. It takes only 2.4 years for the radial bentonite protection to be 95% saturated while it takes 7.6 years to be 99% saturated. The entire buffer is 95% saturated after 6.7 years while it takes 10.5 years to be 99% saturated.

In calculation Stress_1b an external water pressure of 5 MPa has been applied to the rock, which yields a very fast saturation. It takes between 1.5 and 6 years for the buffer to be saturated depending on the definition.

Some results of calculation Stress_2a are shown in Figs 7-7 to 7-11. Figs 7-7 and 7-8 show the distribution of the degree of saturation in the buffer at different times. Most of the buffer is less than 85% saturated after as much as 32 years. Fig 7-9 shows the pore water pressure in the rock after 8 years. A very high negative pore pressure has reached a large part of the rock with negative pore pressure higher than 5 MPa several meters into the rock. This is caused by the low hydraulic conductivity of the rock that cannot supply the buffer with the required amount of water, which results in that the high suction of the buffer is spread into the rock. Fig 7-10 has two diagrams. One of them shows the distribution of the degree of saturation along the radial line on the top of the canister at different times. The other one shows the displacement of the canister and the displacement of the centre of the boundary between the buffer and the backfill as a function of time. The displacements of both the canister and the backfill are not finished after 32 years. Fig 7-11 shows the degree of saturation of equidistant points along the radial line on the top of the canister. The buffer on top of the canister is only 70% saturated after 32 years.

7.3.2   Influence of external water pressure

The influence of the outer water pressure is investigated for 4 cases, where 0 kPa and 5000 kPa have been applied in different calculations at otherwise identical conditions.

*   Stress_1 and 1b (with highly permeable rock) yield that the saturation process goes much faster when 5 MPa is applied (25-60% reduction in time to saturation).

*   Stress_2a and 2b (with very low permeable rock and backfill) yield that the rate of saturation increases when 5 MPa is applied but these calculations have not been run to complete saturation.

*   Stress_3a and 3b1 (fracture free rock without damaged zone) yield that the time until saturation decreases with about 20-50% if 5 MPa is applied. Fig 7-12 shows the degree of saturation in the buffer after 8 years for the two conditions. Fig 7-13 shows the degree of saturation as a function of time for some points in the buffer on

the canister lid. The last figure shows that the largest influence on the saturation rate takes place at a high degree of saturation. The time until complete saturation from 95% to 100% is very lengthy when no water pressure is applied compared to when 5 MPa is applied. The reduction in time to 95% saturation is only about 20% while the reduction is almost 60% at 100% saturation. The reason is that the suction of the buffer is strongly reduced at high degree of saturation, which means that an external water pressure has a higher effect.

• Stress_3a_o and 3b1_o (with de-saturation of the rock) yield similar results as the previous comparison.

The conclusion from these comparisons is that the influence of a high external water pressure of 5MPa reduces the time until saturation with 20% to 60% depending on the conditions and the definition of saturation. If complete saturation (99%-100%) is required the influence is stronger than if 95% is required.

7.3.3   Influence of a damaged zone

The influence of the existence of a damaged zone in the rock surface of the deposition hole is investigated for 4 different conditions. The case with a 1 cm thick zone with an increased hydraulic conductivity (with a factor of 100) has been compared with the case that there is no damaged zone at otherwise identical conditions.

• In calculations Stress_3b1 and 3b2 (no fractures) a damaged zone reduces the time until saturation with up to 13%. The damaged zone supplies the buffer with water to some extent, but the negative pore water pressure is still very high in the rock around the deposition hole (~10 MPa).

• Stress_3b1_o and 3b2_o (no fractures, de-saturated rock) yield similar results as the above. The time until saturation decreases with up to 20% if there is a damaged zone. Fig 7-14 shows the degree of saturation in the buffer after 8 years for the two conditions. Fig 7-15 shows the degree of saturation as a function of time for some points in the buffer on the canister lid.

• In calculations Stress2_3b1 and 2_3b2 (with fractures) the damaged zone reduces the time until saturation with up to 27%. The fractures reduce the pathway of water through the rock and the damaged zone but the negative pore pressure is still very high near the rock surface (almost 10 MPa).

• In calculations Stress2_3b1_o and 2_3b2_o (with fractures and de-saturated rock) we can expect the largest effect of the damaged zone, since the hydraulic conductivity of the rock is reduced when it is de-saturated. However, the damaged zone is also de-saturated, which limits the effect to up to 35%. Fig 7-16 shows the degree of saturation in the buffer after 2 years for the two conditions. The influence of the two fractures is obvious, since the buffer is saturated between the central fracture and the canister for both cases. The increased rate of saturation outside the fractures is also clearly seen.

The conclusion from these calculations is that a damaged zone increases the rate of saturation, but the increase is limited to less than 35% for the cases studied in spite of that the damaged zone has been assumed to have 100 times higher hydraulic conductivity than the rock matrix.

7.3.4   Influence of fractures

The influence of the existence of fractures in the rock intersecting the deposition hole is investigated for 4 different conditions at otherwise identical conditions.

- In calculations Stress_3b1 and 2_3b1 (saturated rock and no damaged zone) the two fractures reduce the time until saturation with up to 14 %.

- Stress_3b1_o and 2_3b1_o (de-saturated rock and no damaged zone) yield a stronger reduction. The time until saturation decreases with up to 22% if there are two fractures. Figs 7-17 to 7-19 show the degree of saturation in the buffer after 1, 4, and 8 years for the two conditions. The strong influence from the fractures is clearly seen. The pore pressure in the rock after 4 years is compared in Fig 7-20. The two fractures lead the high water pressure into the intersection with the deposition hole, but the pressure is reduced and turns to high negative values that de-saturate the rock within less than a meter from the fracture.

- In calculations Stress_3b2 and 2_3b2 (saturated rock and damaged zone) the reduction in time until saturation is up to 26%.

- In calculations Stress_3b2_o and 2_3b2_o (de-saturated rock and damaged zone) the influence of the fractures is strong with a reduction in time to saturation of up to 28 %

The conclusion from these comparisons is that two horizontal fractures that intersect a deposition hole in the described configuration will increase the rate of saturation, although the influence is rather limited due to the long distance between the fractures. If the rock is de-saturated the effect is stronger. The influence of fractures is especially strong with a decrease in time to 95% saturation at the radial periphery of the canister of up to 28% when there is a disturbed zone.

The effect is of course strongly related to the hydraulic conductivity of the rock matrix. In the presented calculations the hydraulic conductivity of the rock matrix is 10^{-13} m/s. If the hydraulic conductivity is higher the flow from the matrix may be predominant and the effect of fractures will be lower. On the other hand if there are more than two fractures that intersect the hole the effect will be stronger.

7.3.5   Influence of de-saturated rock

The influence of the ability of the rock to de-saturate is investigated for 5 different conditions at otherwise identical conditions.

- In calculations Stress_3a and 3a_o (no water pressure, no fractures, and no damaged zone) de-saturation of the rock has a very strong influence. The time until saturation is extended with up to 86%. Fig 7-21 shows the degree of saturation of the buffer as a function of time at a radial section in the centre of the canister for the two cases. The de-saturation also strongly influences the pore water pressure distribution in the rock, which is shown in Fig 7-22. De-saturation, which takes place when the negative water pressure becomes higher than 1 MPa ($u < -1$ MPa), is limited to about 1 m into the rock, while it reaches several meters into the rock if de-saturation is not taken into account.

- Stress_3b1 and 3b1_o (no fractures and no damaged zone) yield that de-saturated rock causes up to 50% longer time until saturation.

- In calculations Stress_3b2 and 3b2_o (damaged zone, no fractures) the time until saturation is extended with up to 15%.

- In calculations Stress2_3b1 and 2_3b1_o (fractures but no damaged zone) the influence of the de-saturated rock extend the time until saturation of the buffer of up to 25%.

- Stress2_3b2 and 2_3b2_o (fractures and damaged zone) yield an insignificant influence of de-saturation in the rock (up to 9%). The reason seems to be that the fractures and the disturbed zone dominate the water transport, so that the processes in the rock matrix are less important.

The conclusion from these comparisons is that de-saturation in the rock may be important for the saturation rate in the buffer if the rock matrix has a low hydraulic conductivity and if there is no external water pressure in the rock. The influence is also strongest for the time to 95% saturation at the radial canister periphery. The influence is smaller when a few fractures supply the buffer with water in combination with a damaged zoned and high external water pressure.

7.3.6 Influence of fracture transmissivity

The influence of the transmissivity of the fractures is investigated for 3 different cases at otherwise identical conditions (no damaged zone, 5 MPa water pressure, and de-saturation of the rock).

The two fractures intersecting the deposition hole have been given three different hydraulic conductivity values (K). These values can be recalculated to transmissivity (T) according to Eqn 7-2 and (with 5 MPa water pressure at the boundary) to a rough estimate of the total inflow into the deposition hole (Q) before deposition according to Eqn 7-3.

$$T = Kd \qquad (7-2)$$

$$Q = 2\pi T(h_2 - h_1)/\ln(r_2/r_1) \qquad (7-3)$$

where

T = transmissivity (m²/s)

K = hydraulic conductivity (m/s)

d = fracture thickness in the model (= 0.01 m)

Q = total inflow into the hole (m³)

h_2-h_1 = pressure drop between the radial boundary and the hole (= 500 mwh)

r_2 = outer radius of the rock (=11.0 m)

r_1 = radius of the hole (= 0.875 m)

Table 7-2 shows the fracture properties used in the three calculations.

Table 7-2. Fracture properties

Calculation	K (m/s)	T (m²/s)	Q (l/hours)
Stress2_3b1_o	10^{-8}	10^{-10}	0.45
Stress2_3b1_oa	10^{-7}	10^{-9}	4.5
Stress2_3b1_ob	10^{-9}	10^{-11}	0.045

The results of theTHM calculations are illustrated by Fig 7-23, where the degree of saturation is plotted as a function of time for the two calculations that have the fracture transmissivity 10^{-9} and 10^{-11} m²/s. The figure shows that the results are identical and that even low permeable fractures may provide the buffer with sufficient amount of water. The results also show that the total inflow into the empty deposition hole may have a very small influence on the rate of saturation.

Denote that the fractures are idealised two-dimensional. The influence of a variation in transmissivity in the third dimension is not investigated. It is though likely that the spreading of the wetting is the same in that direction and that the delay caused by channel flow is limited when the flow rate in the channel is large enough to supply the bentonite with the requested amount of water.

7.3.7 A typical example of the water saturation process

The last calculation (Stress2_3b1_ob) will be used to illustrate a typical example of the conditions in a deposition hole. It includes a rock matrix with the hydraulic conductivity 10^{-13} m/s, no damaged zone, two fractures which yield an inflow into the empty deposition hole of 0.044 l/h, a boundary water pressure of 5 MPa 10 m outside the hole and possibility to de-saturate the rock.

Figs 7-24 and 7-25 show the degree of saturation in the buffer at different times. Water is supplied from the rock matrix but particularly from the fractures and the backfill. Fig 7-26 shows the pore water pressure in the rock. The water pressure is lower than -1MPa,

and thus de-saturated, about 0.5 m into the rock between the fractures. The high water pressures in the fractures extend all the way to the deposition hole, which shows that the water supply through the fractures and the backfill is strong. The degree of saturation as a function of time in the buffer at the lid of the canister is shown in Fig 7-27. Drying before wetting takes place in most parts of the buffer. The displacements of the canister and the interface between the buffer and the backfill are shown in Fig 7-28. It is interesting to note that the displacements continue a long time after completed water saturation.

The radial total stress in the buffer material at different times is shown in Figs 7-29 and 7-30. The total stress is the sum of the effective stress (swelling pressure) and the pore water pressure. Some interesting observations can be done:

- The total stress increases rather fast in the entire buffer and the pressure is a few MPa already after 1 year

- Further increase in pressure follows the water saturation process, which means that the pressure is inhomogeneous and much higher at the fracture intersections.

- The pressure is not stabilised until long time after completed saturation due to the upward swelling

- The pressure distribution is rather homogeneous after equilibrium, except for above the canister, where it is considerably lower due to the swelling

Observe that the mechanical part of the modelling is incomplete since the difference in initial density between the blocks and the outer slot is not considered and thus the radial swelling of the blocks and corresponding compression of the slots are not modelled.

8 Conclusions

The results of the calculations show that the influence of most changes in rock properties and boundary conditions are rather large. The following general conclusions are drawn from the calculations, although the conclusions must be preliminary, since there is a lack in knowledge of the hydraulic behaviour of the rock and the rock/buffer interface. Furthermore the model of the buffer material is not satisfactory.

A highly permeable rock with $K = 10^{-10}$ m/s yields that the buffer between the canister and the periphery of the hole is highly saturated within a few years, while it takes up to 10 years to get complete saturation in the entire buffer if the water pressure in the surrounding rock is low. These results are expected to be typical when the hydraulic conductivity is much higher in the rock than in the buffer. When the rock is less or equally permeable as the buffer the wetting is delayed by the flow resistance of the rock.

When water pressure corresponding to hydrostatic at the depth 500 m is present in a boundary 10 m from the deposition hole the rate of wetting is increased considerably (20%-60% reduction in time to saturation), especially at the end of the wetting process.

When there is a 1 cm thick damaged zone with a hydraulic conductivity that is 100 times higher than the rock matrix at the surface of the deposition hole, the time until saturation is reduced up to 35%. The strongest effect is reached when the rock is allowed to de-saturate.

De-saturation in the rock may be important for the saturation rate in the buffer if the rock matrix has a low hydraulic conductivity and if there is no external water pressure in the rock. The influence is strongest for the time to 95% saturation at the radial canister periphery where up to 86% extension of the saturation period was reached. The influence is smaller when a few fractures supply the buffer with water in combination with a high external water pressure. A better knowledge of the de-saturation properties of the rock is required before definitive conclusions can be drawn.

Two horizontal fractures that intersect a deposition hole in the described configuration will increase the rate of saturation, although the influence is rather limited due to the long distance between the fractures. If the rock is de-saturated the effect is stronger. The influence of fractures is especially strong at the radial periphery of the canister with a decrease in time to 95% saturation of up to 28% when there is a disturbed zone

When the transmissivity of the fractures is changed from 10^{-9} to 10^{-11} m^2/s, which corresponds to an inflow of 4.4 and 0.044 l/h into the hole, no change in wetting rate could be observed. The buffer can obviously not utilise the water supplied by large fractures.

39

References

/2-1/   **Hibbitt, Karlsson, and Sorensen** - ABAQUS manuals, HKS Inc.

/3-1/   **Börgesson L. & Johannesson L.-E. 1995.** Thermo-Hydro-Mechanical modelling of water unsaturated buffer materials. Status 1995. SKB Arbetsrapport AR 95-32.

/5-1/   **Börgesson L, Johannesson L-E, Sandén T, Hernelind J, 1995.** Modelling of the physical behaviour of water saturated clay barriers. Laboratory tests, material models and finite element application. SKB Technical Report TR 95-20, SKB, Stockholm.

/5-2/   **Börgesson L., Fredriksson A. & Johannesson L.-E. 1994.** Heat conductivity of buffer materials. SKB Technical Report TR 94-29.

/7-1/   **Hökmark H. 1996.** Canister Positioning - Stage 1 – Thermomechanical Nearfield Rock Analysis. SKB, Djupförvar, AR D-96-014.
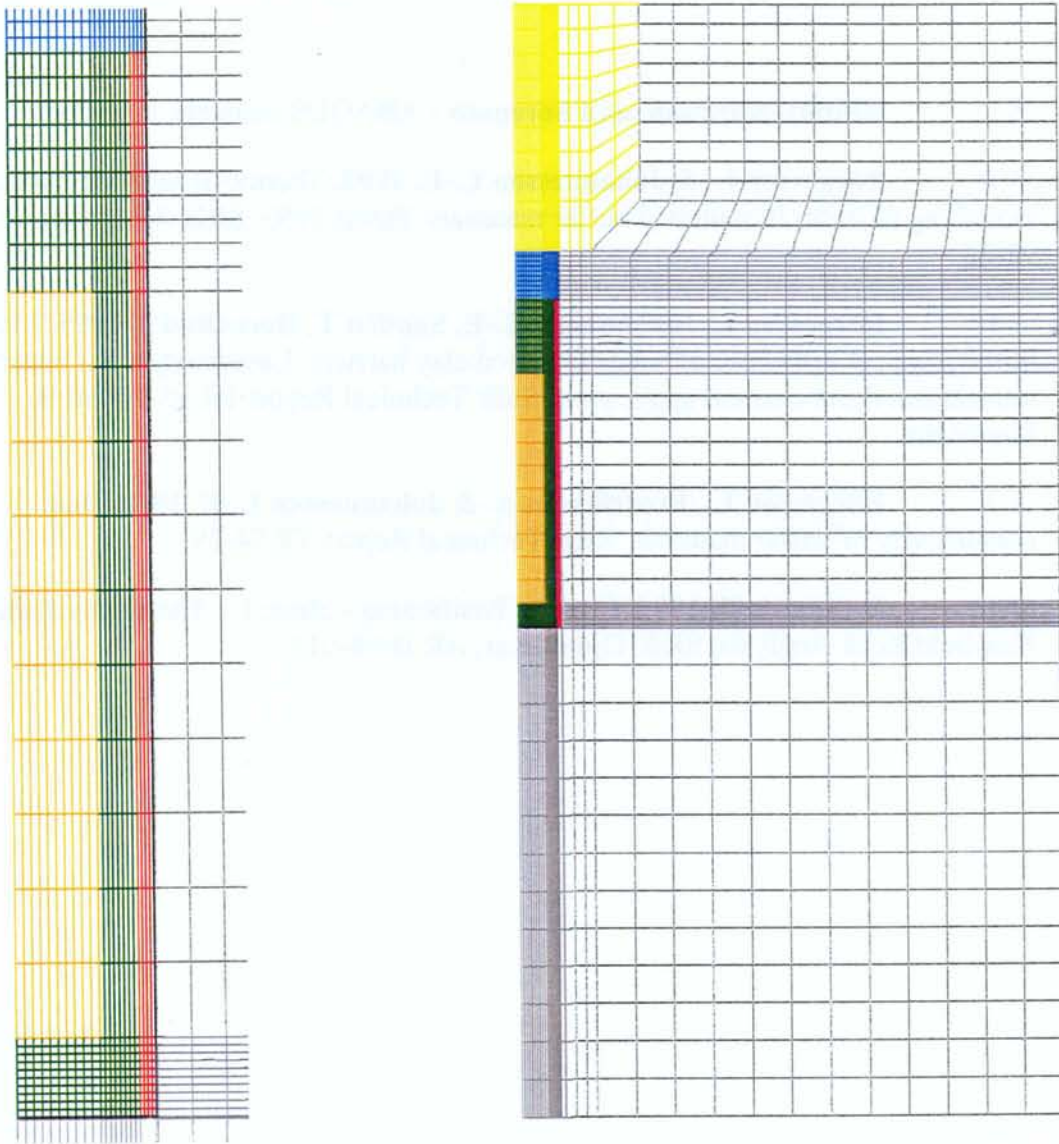
Rock: *grey*

Backfill: *yellow and blue*

Buffer: *green and red*

Canister: *yellow*

Disturbed zone: *black line*

Figure 4-1. The entire element mesh and an enlargement of the deposition hole (axial symmetry).
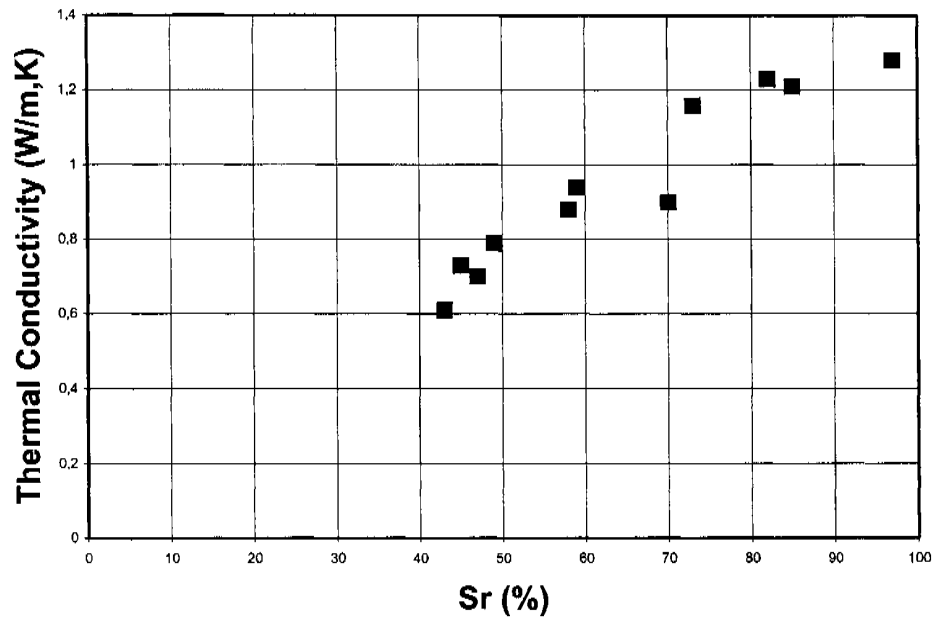
Figure 5-1. Measured thermal conductivity as a function of degree of saturation
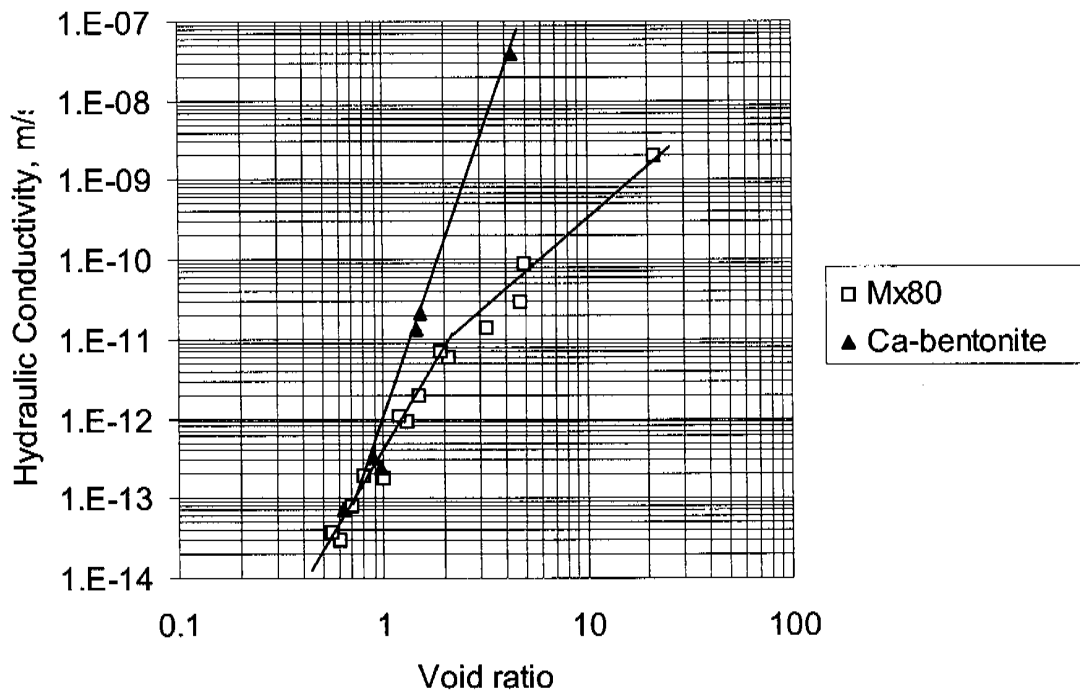
Figure 5-2. Measured hydraulic conductivity at different void ratios
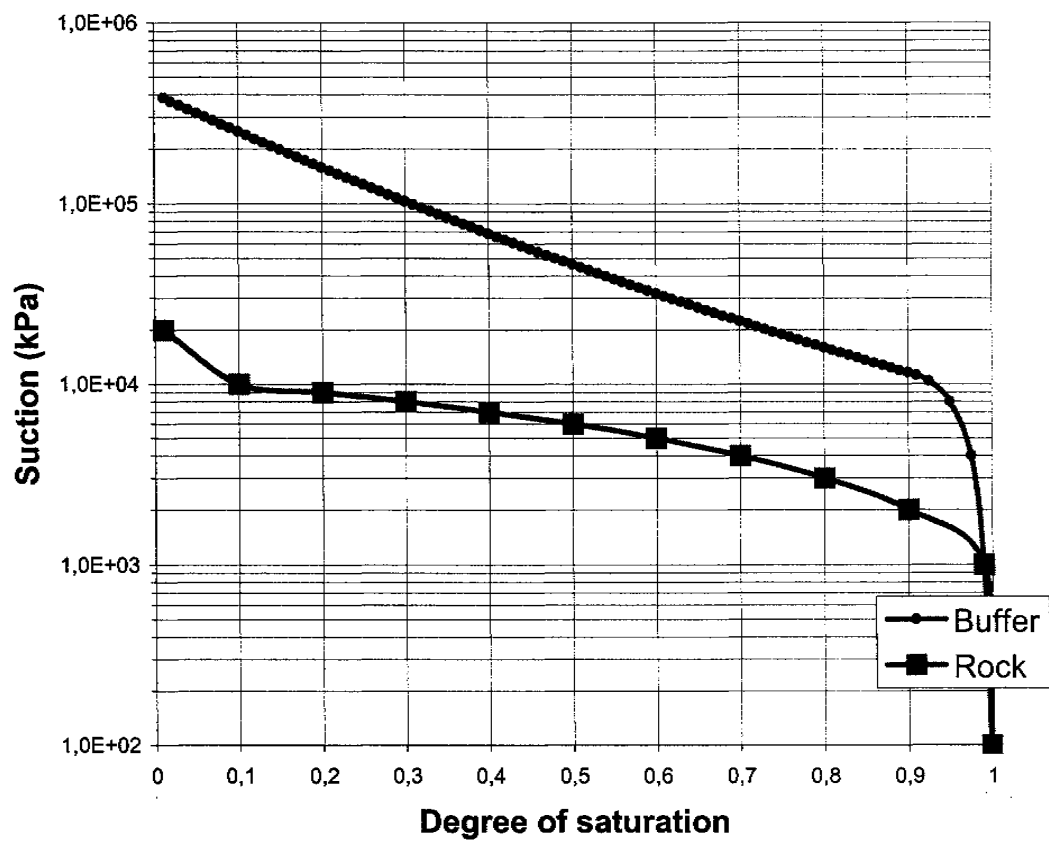
Figure 5-3. Relation between suction and degree of saturation used in the material models of the buffer material and the rock
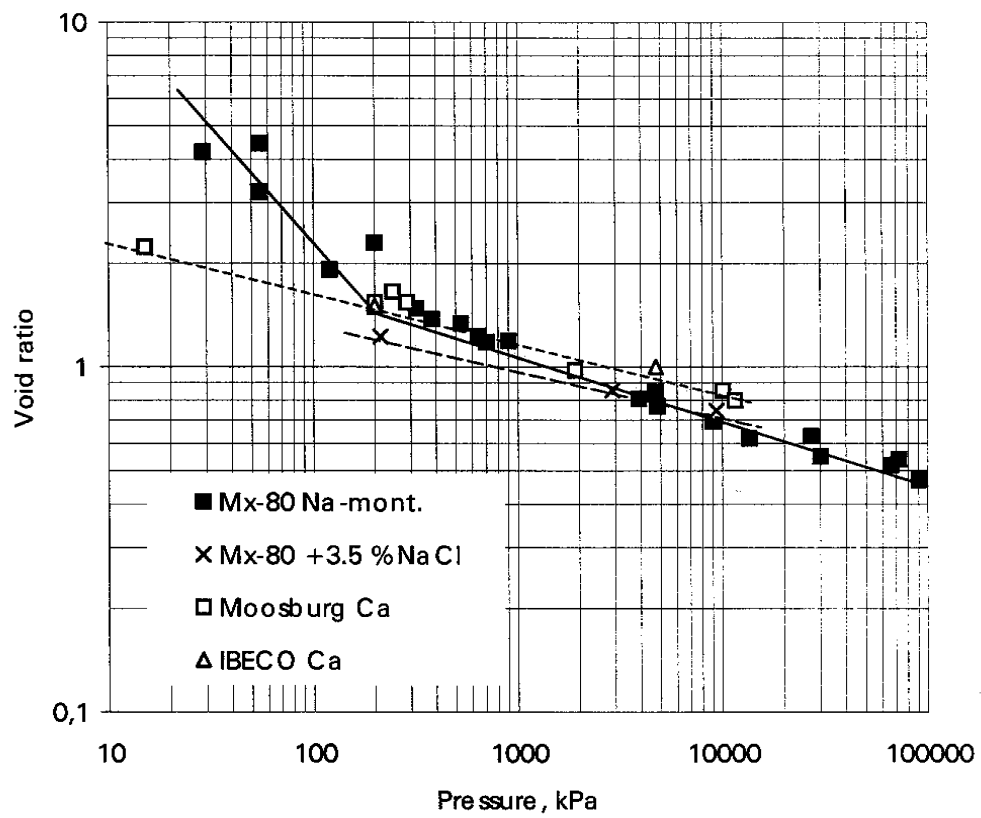
Figure 5-4. Results from swelling pressure tests
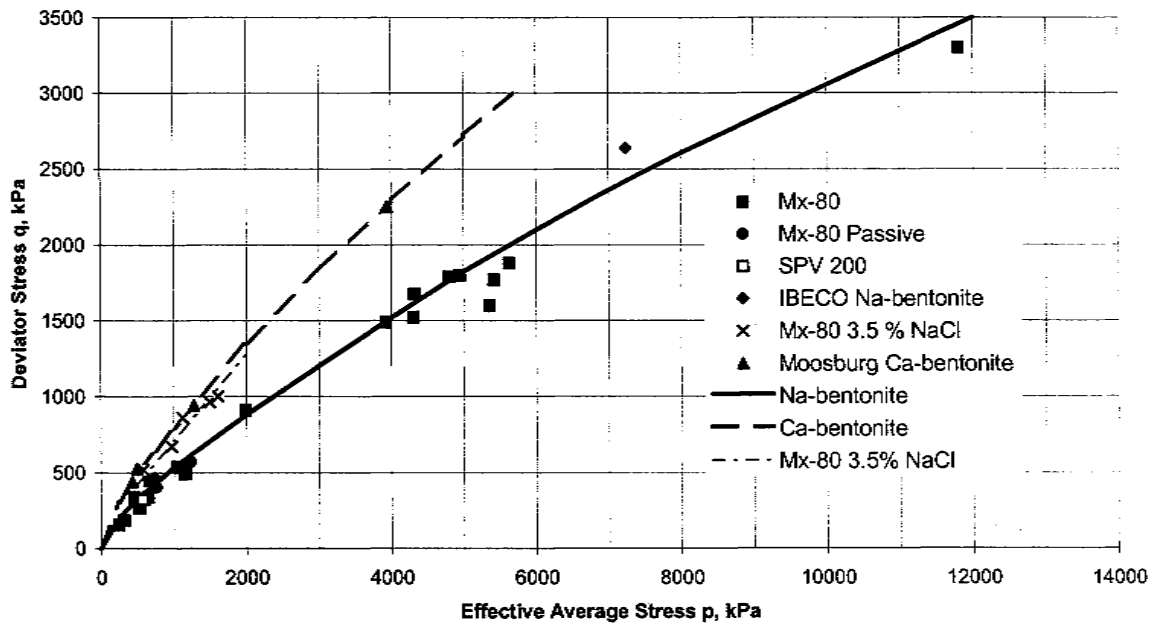
Figure 5-5. Triaxial test results
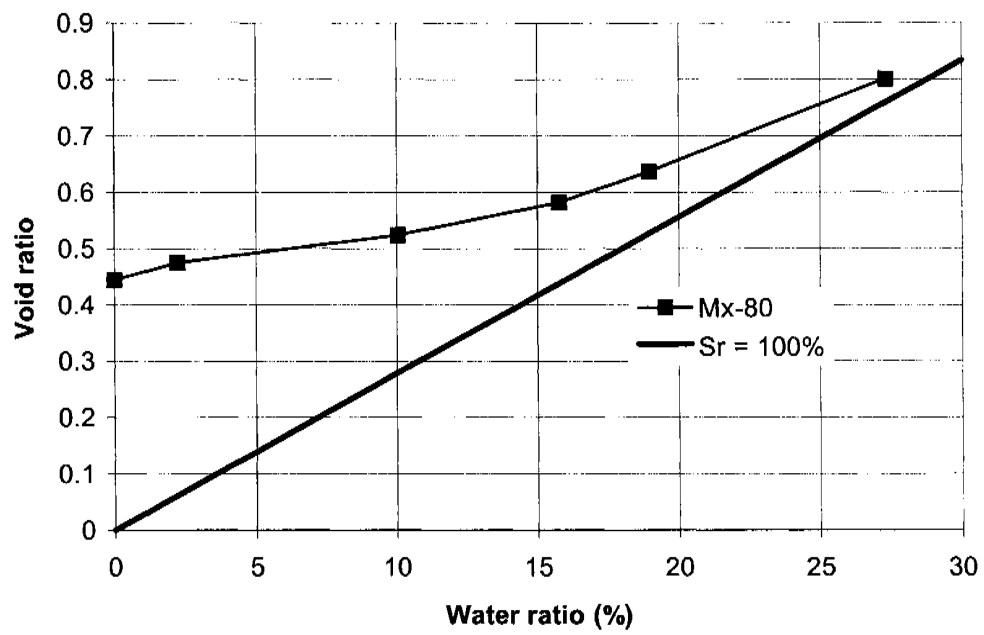
Figure 5-6. Results of drying tests on MX-80
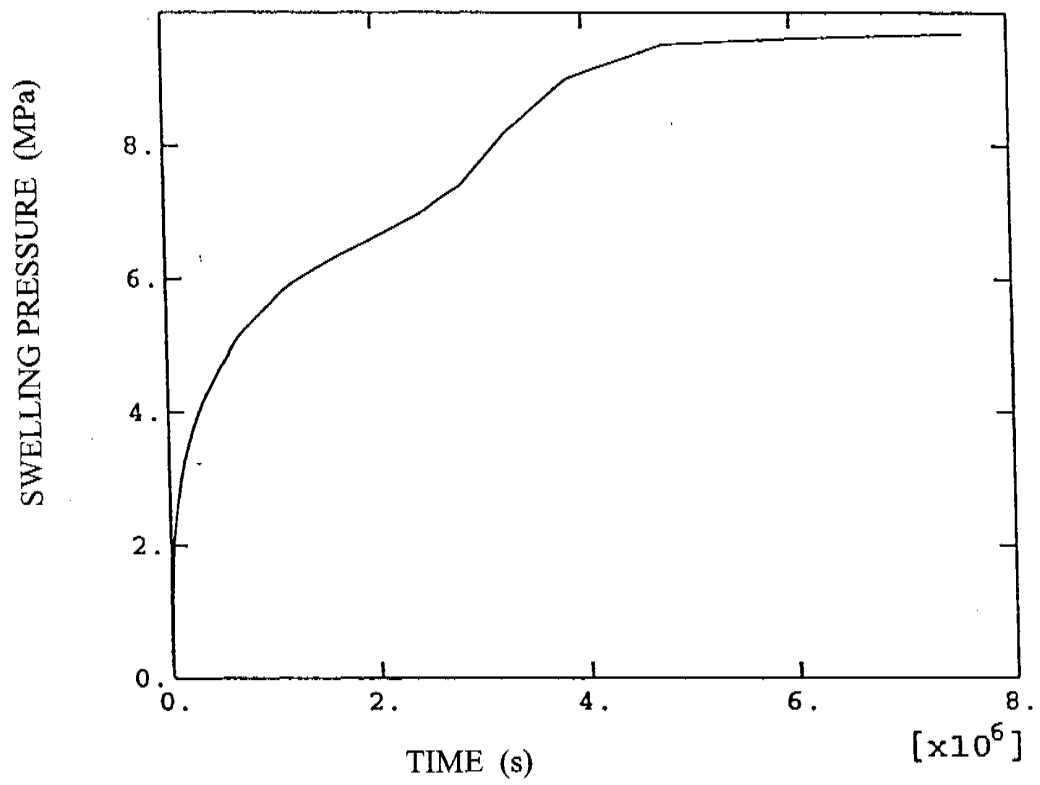
Figure 5-7. Calculated swelling pressure (MPa) as a function of time (s) for a simulated water uptake test. $5 \cdot 10^6$ seconds correspond to about 2 months.
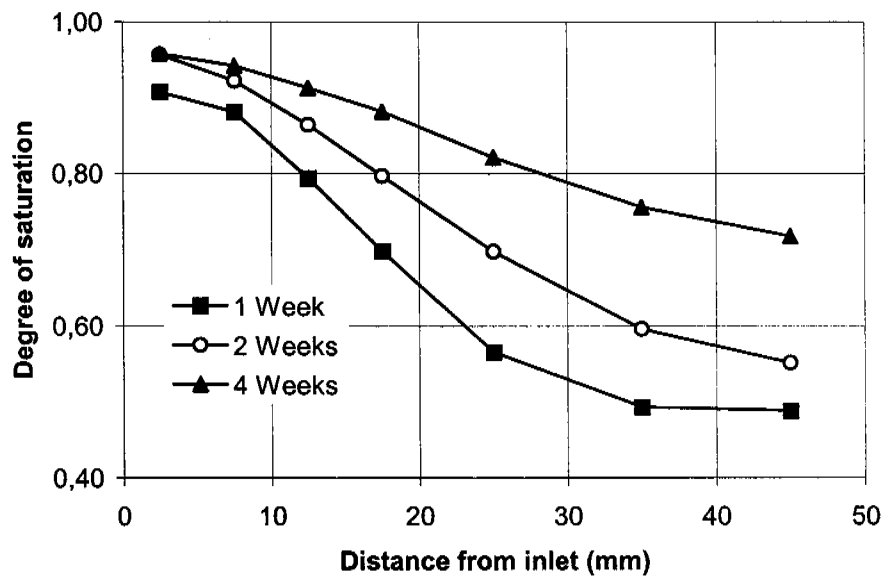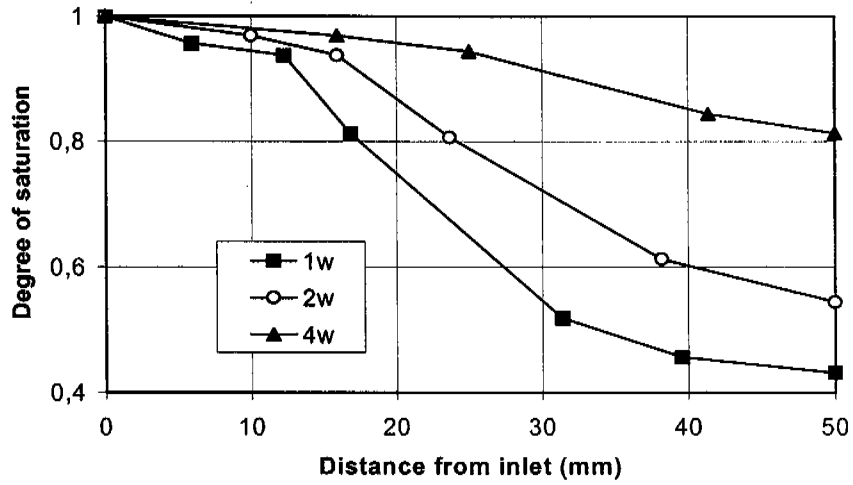
Figure 5-8. Calculated degree of saturation as a function of the distance from the water inlet after 1, 2, and 4 weeks (upper) and corresponding measurements (lower)
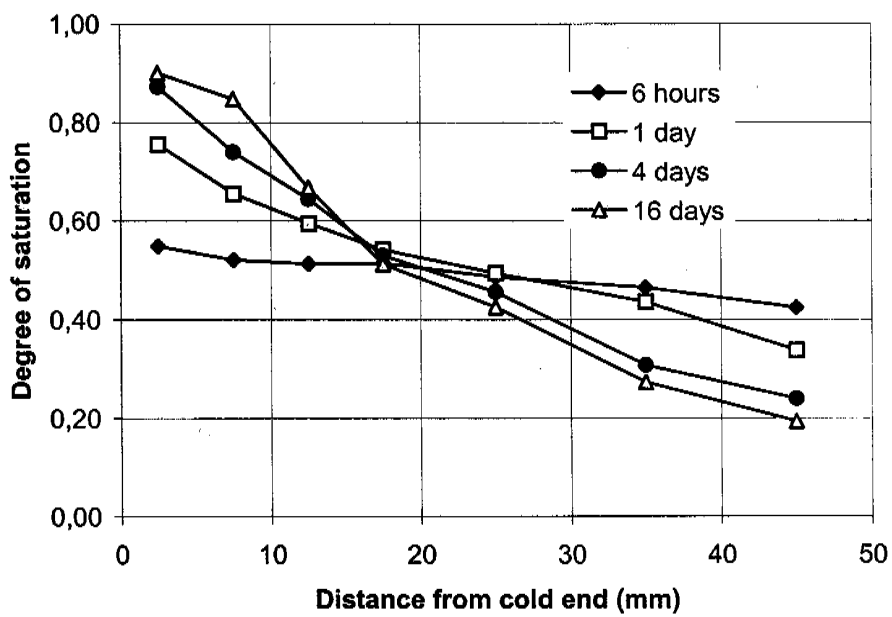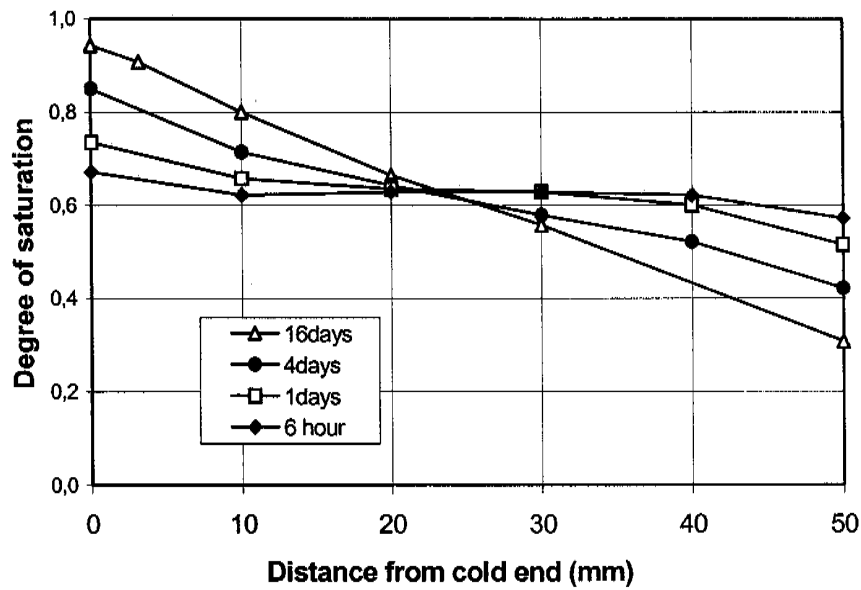
Figure 5-9. Calculated degree of saturation as a function of the distance from the cold end after 0.25, 1, 4, and 16 days (upper) and corresponding measurements (lower)
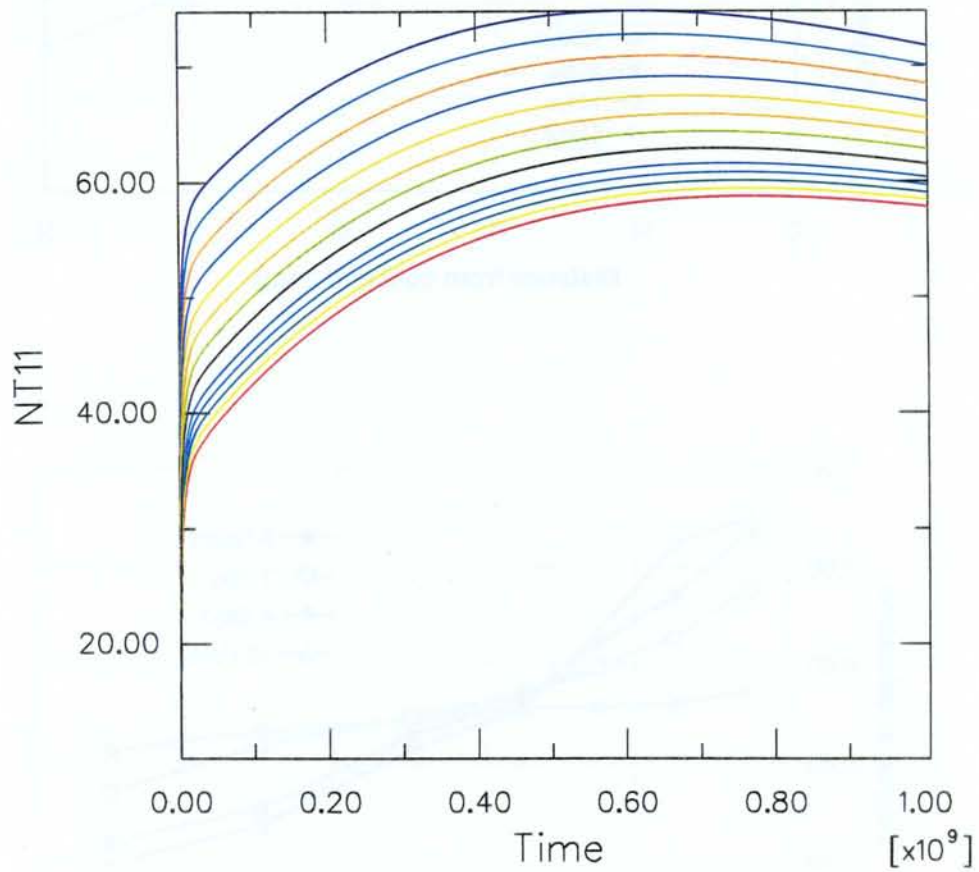
Figure 7-1. Calculated temperature (°C) in the buffer as a function of time (s) for 13 equidistant points at mid height canister from the canister surface (highest temperature) to the rock surface (lowest temperature).
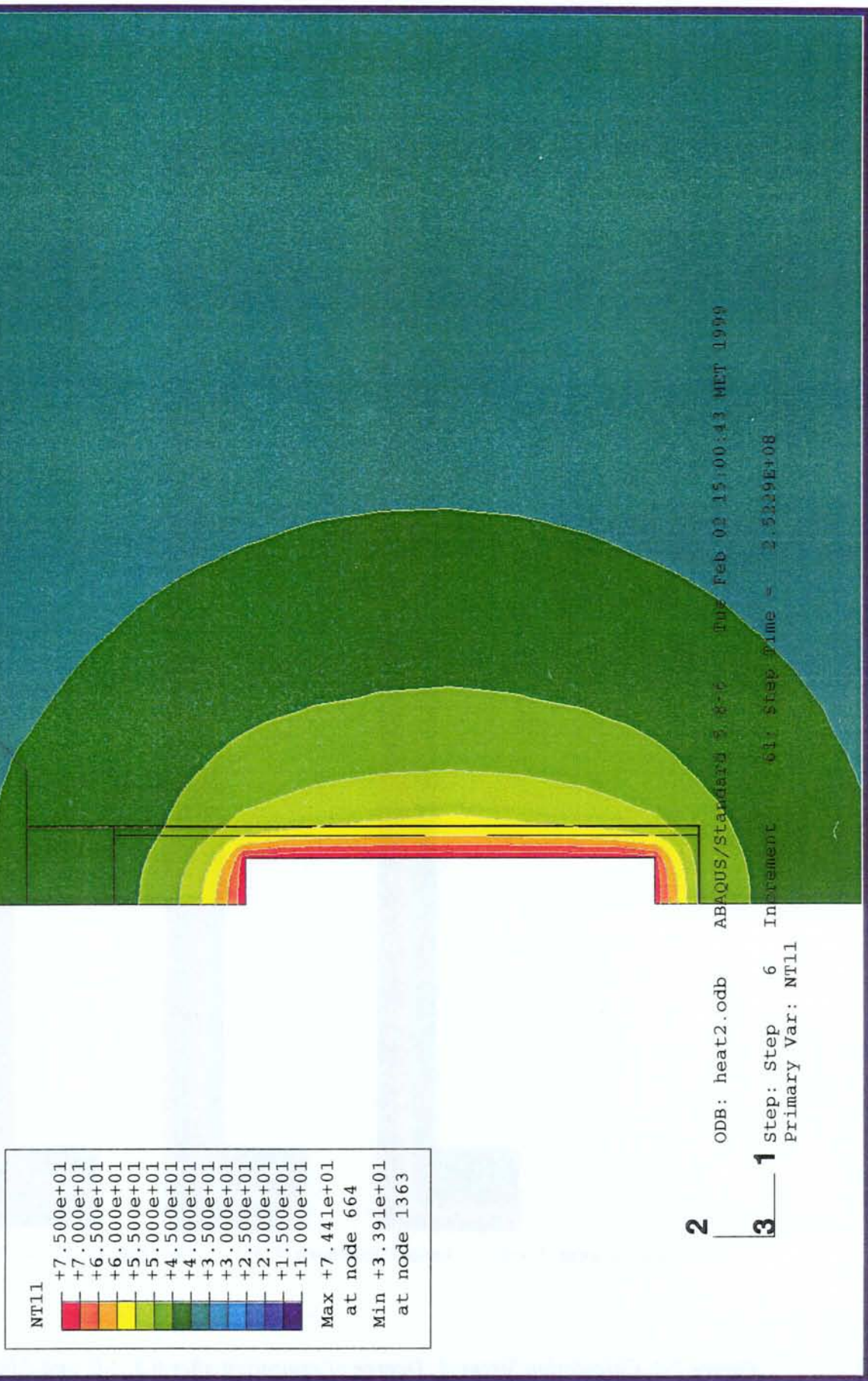
Figure 7-2. Calculated temperature distribution (°C) after 8 years
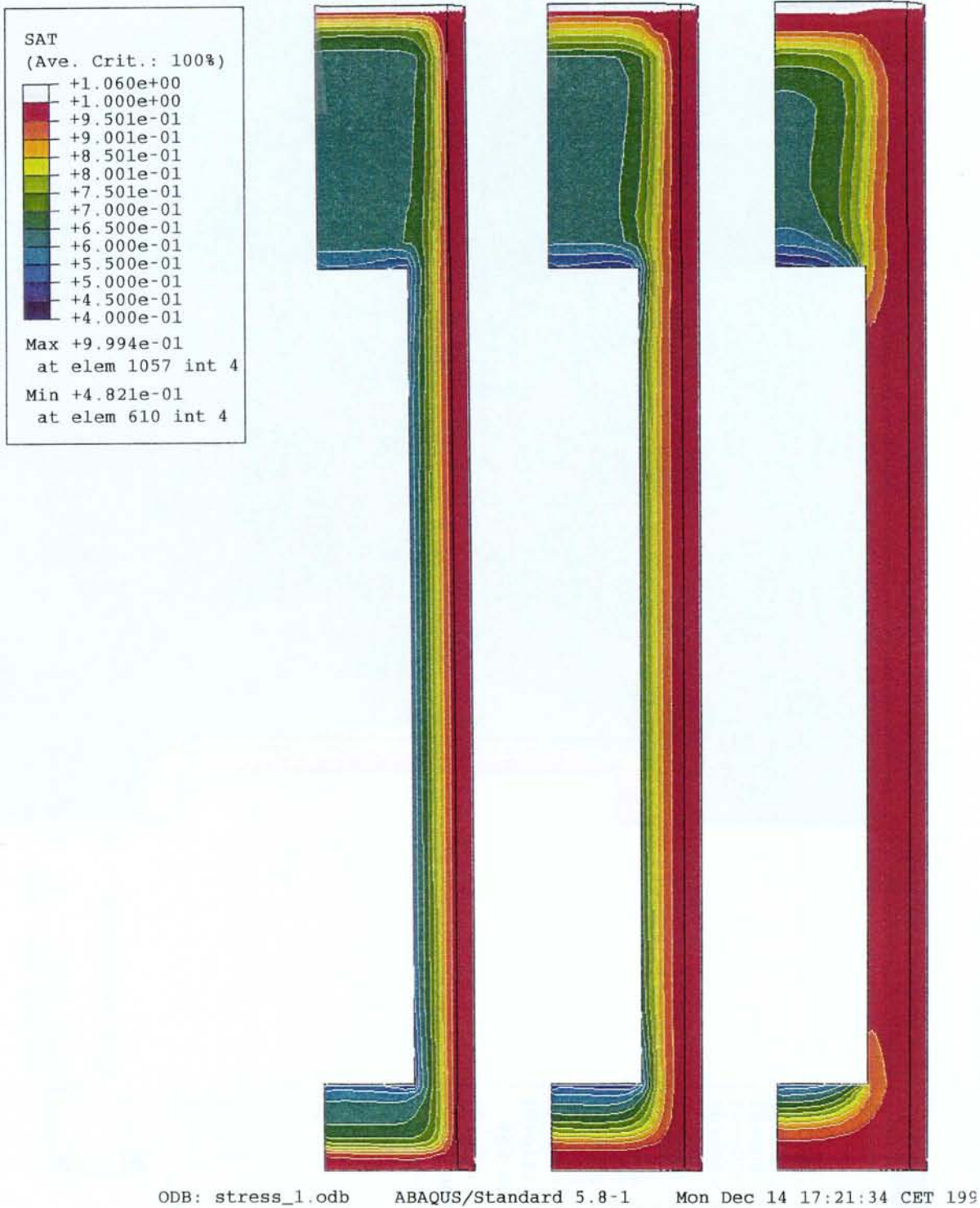
Figure 7-3. Calculation Stress_1. Degree of saturation after 0.5, 1.0, and 2.0 years (left to right)

```
SAT
(Ave. Crit.: 100%)
    +1.010e+00
    +1.000e+00
    +9.501e-01
    +9.001e-01
    +8.501e-01
    +8.001e-01
    +7.501e-01
    +7.000e-01
    +6.500e-01
    +6.000e-01
    +5.500e-01
    +5.000e-01
    +4.500e-01
    +4.000e-01
Max +1.000e+00
  at elem 949 int 3
Min +5.604e-01
  at elem 851 int 3
```

ODB: stress_1.odb   ABAQUS/Standard 5.8-1   Mon Dec 14 17:21:34 CET 199
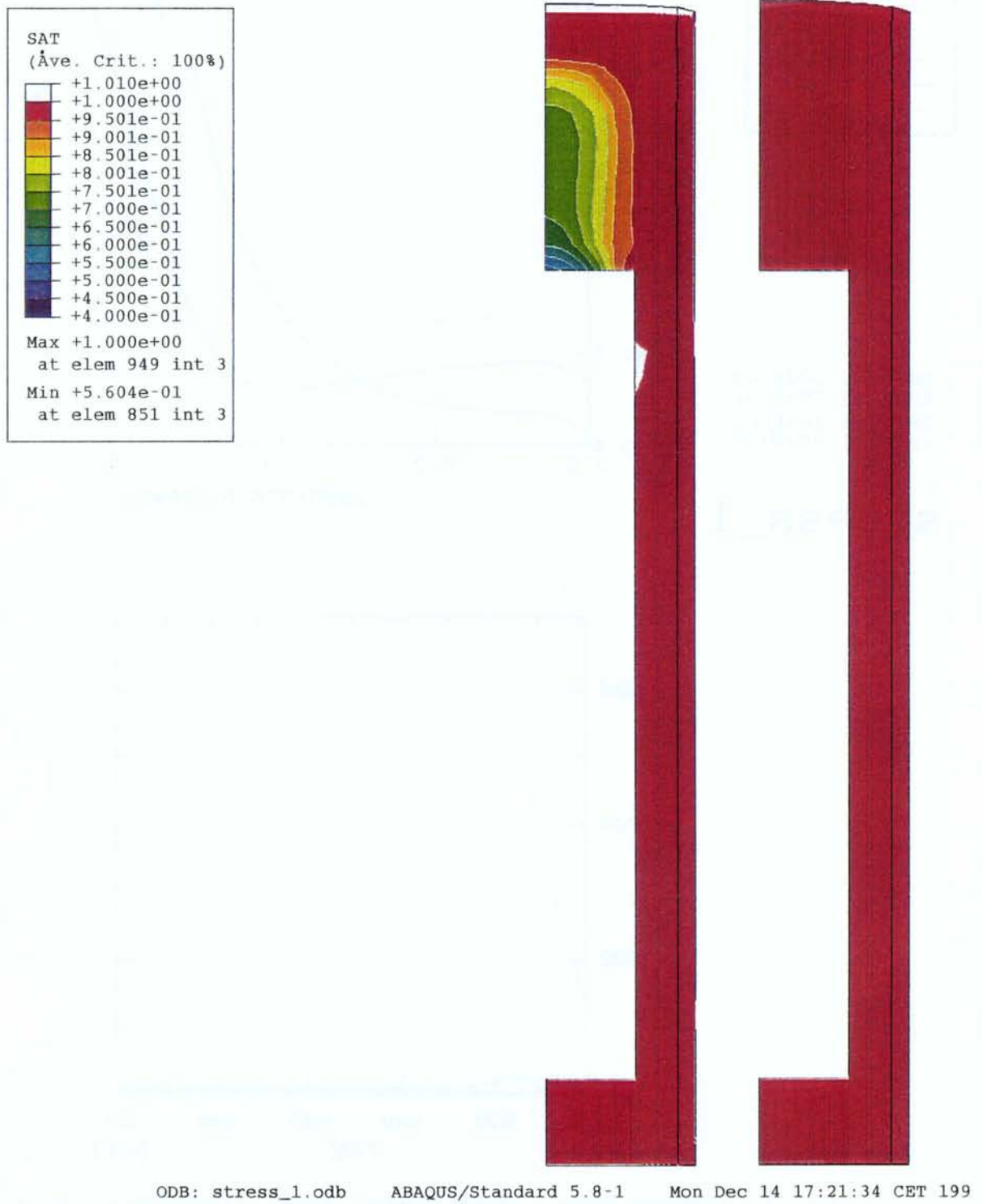
Figure 7-4. Calculation Stress_1. Degree of saturation after 4.0 and 8.0 years (left to right)
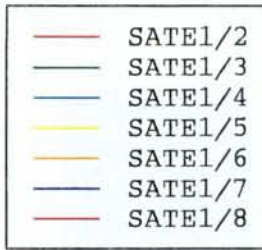
XMIN   0.000E+00
XMAX   8.755E-01
YMIN   4.165E-01
YMAX   1.002E+00
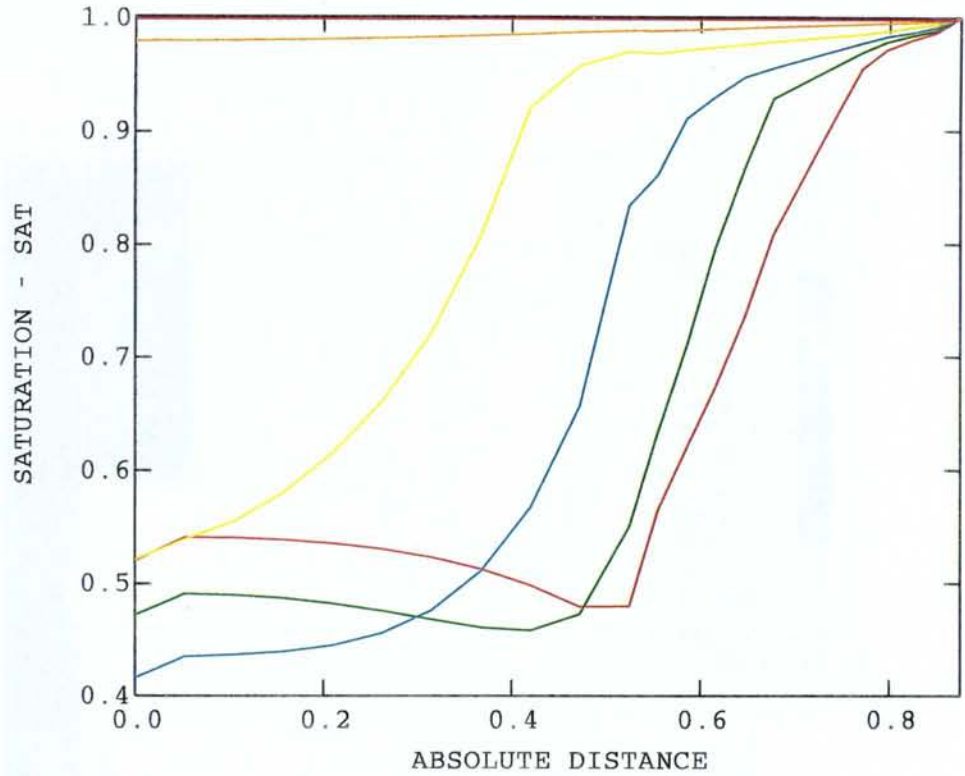
stress_1
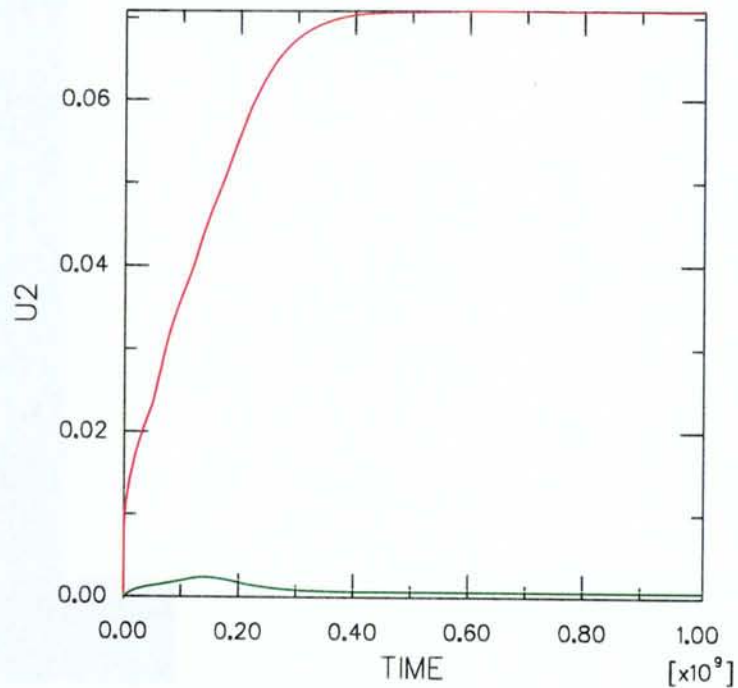
Figure 7-5. Calculation Stress_1. Upper diagram: Degree of saturation as a function of the radial distance from the centre of the canister lid after 0.5 years (/2), 1.0 year (/3), 2.0 years (/4), 4.0 years (/5), 8.0 years (/6), 16.0 years (/7), and 32.0 years (/8) years. Lower diagram: Displacement (m) of the canister (red) and the centre of the boundary between the buffer and backfill (green) as a function of time (s)
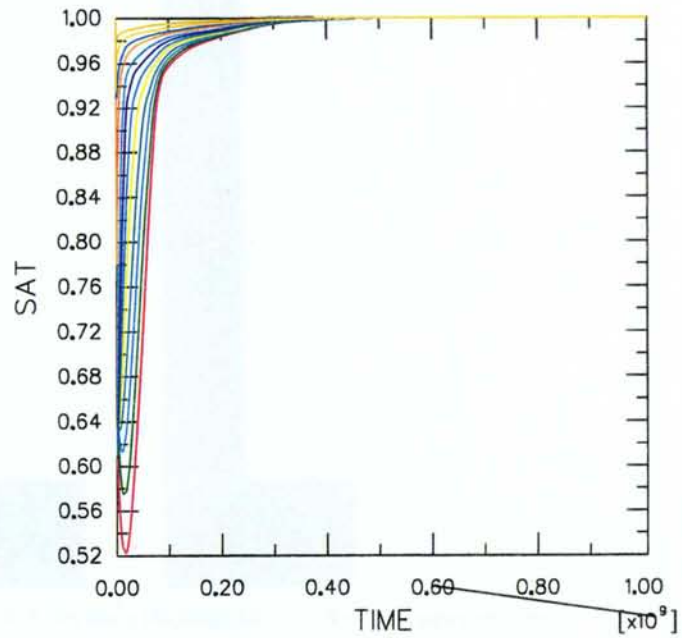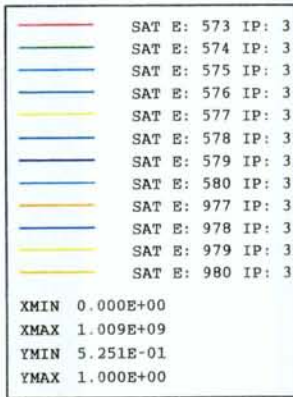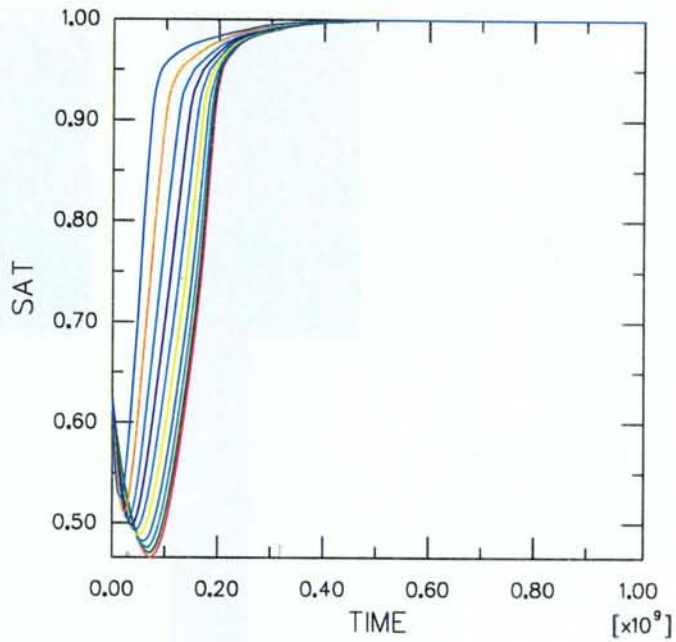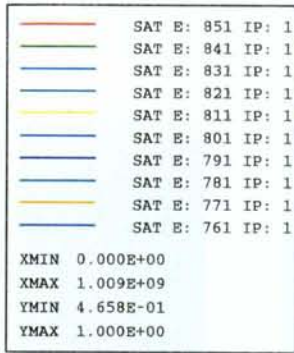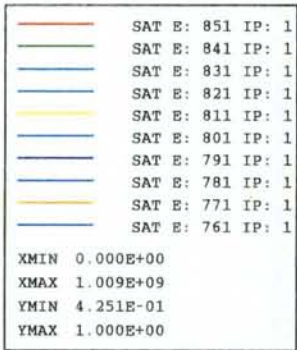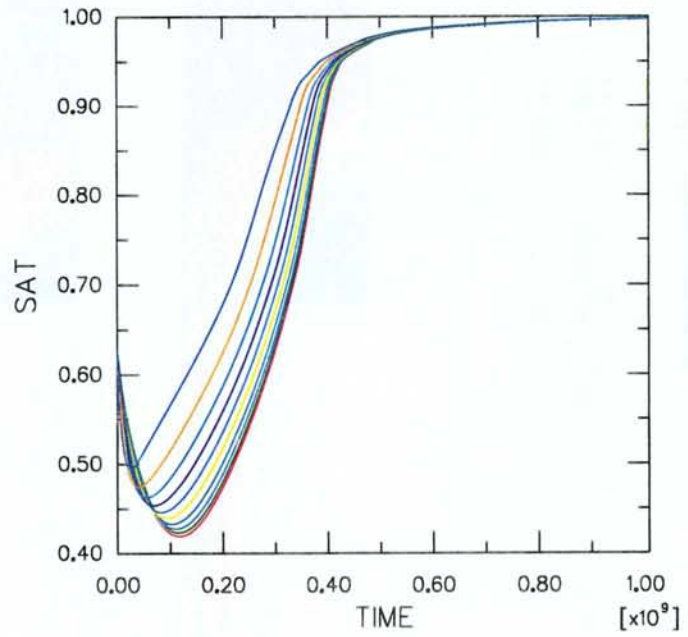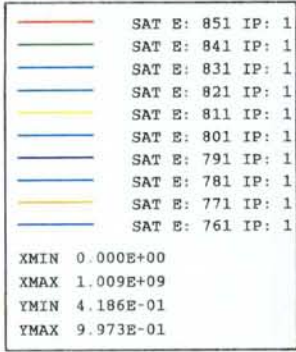
Figure 7-6. Calculation Stress_1. Degree of saturation in the buffer of equidistant points along the radial line on top of the canister as a function of time (s). Upper: From 0 m to 0.525 m (along the canister lid). Lower: From 0.525 m to 0.875 m.

SAT
(Ave. Crit.: 100%)
+1.000e+00
+9.501e-01
+9.001e-01
+8.501e-01
+8.001e-01
+7.501e-01
+7.000e-01
+6.500e-01
+6.000e-01
+5.500e-01
+5.000e-01
+4.500e-01
+4.000e-01
+3.602e-01
Max +9.213e-01
at elem 1060 int 4
Min +3.959e-01
at elem 680 int 4

ODB: stress_2a.odb   ABAQUS/Standard 5.8-1   Mon Dec 14 17:14:07 CET 1!
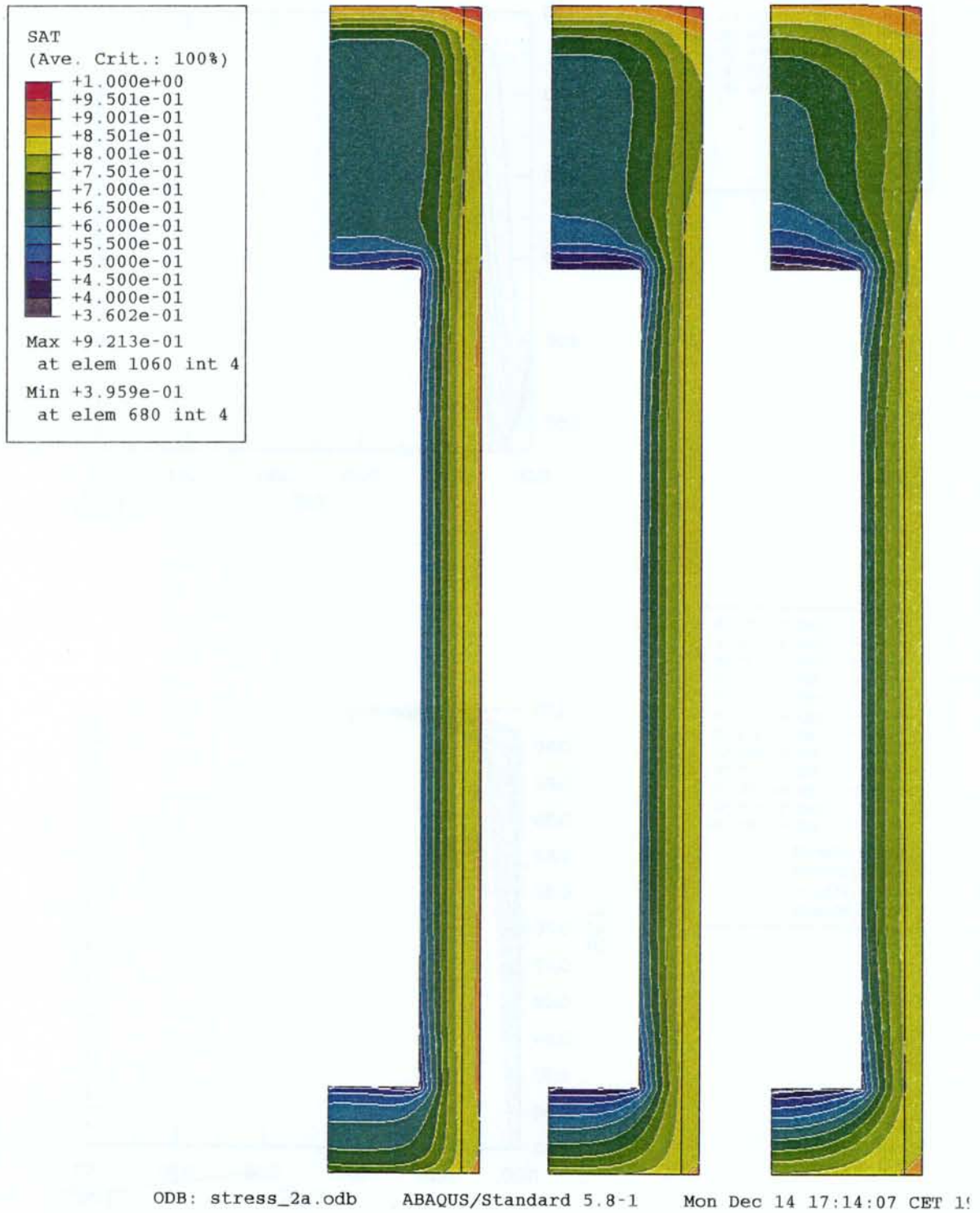
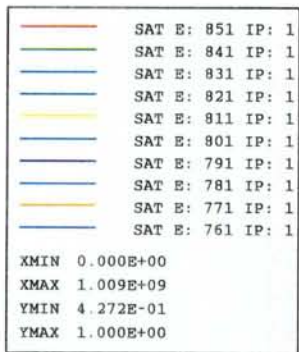Figure 7-7. Calculation Stress_2a. Degree of saturation after 1, 2, and 4 years (left to right)

SAT
(Ave. Crit.: 100%)
+1.000e+00
+9.501e-01
+9.001e-01
+8.501e-01
+8.001e-01
+7.501e-01
+7.000e-01
+6.500e-01
+6.000e-01
+5.500e-01
+5.000e-01
+4.500e-01
+4.000e-01
Max +8.961e-01
  at elem 1060 int 4
Min +5.325e-01
  at elem 851 int 3

ODB: stress_2a.odb   ABAQUS/Standard 5.8-1   Mon Dec 14 17:14:07 CET

Figure 7-8. Calculation Stress_2a. Degree of saturation after 8, 16, and 32 years (left to right)

58

POR
+0.000e+00
-5.833e+02
-1.167e+03
-1.750e+03
-2.333e+03
-2.917e+03
-3.500e+03
-4.083e+03
-4.667e+03
-5.250e+03
-5.833e+03
-6.417e+03
-7.000e+03
-1.583e+04

Max +0.000e+00
at node 1350
Min -1.583e+04
at node 1587
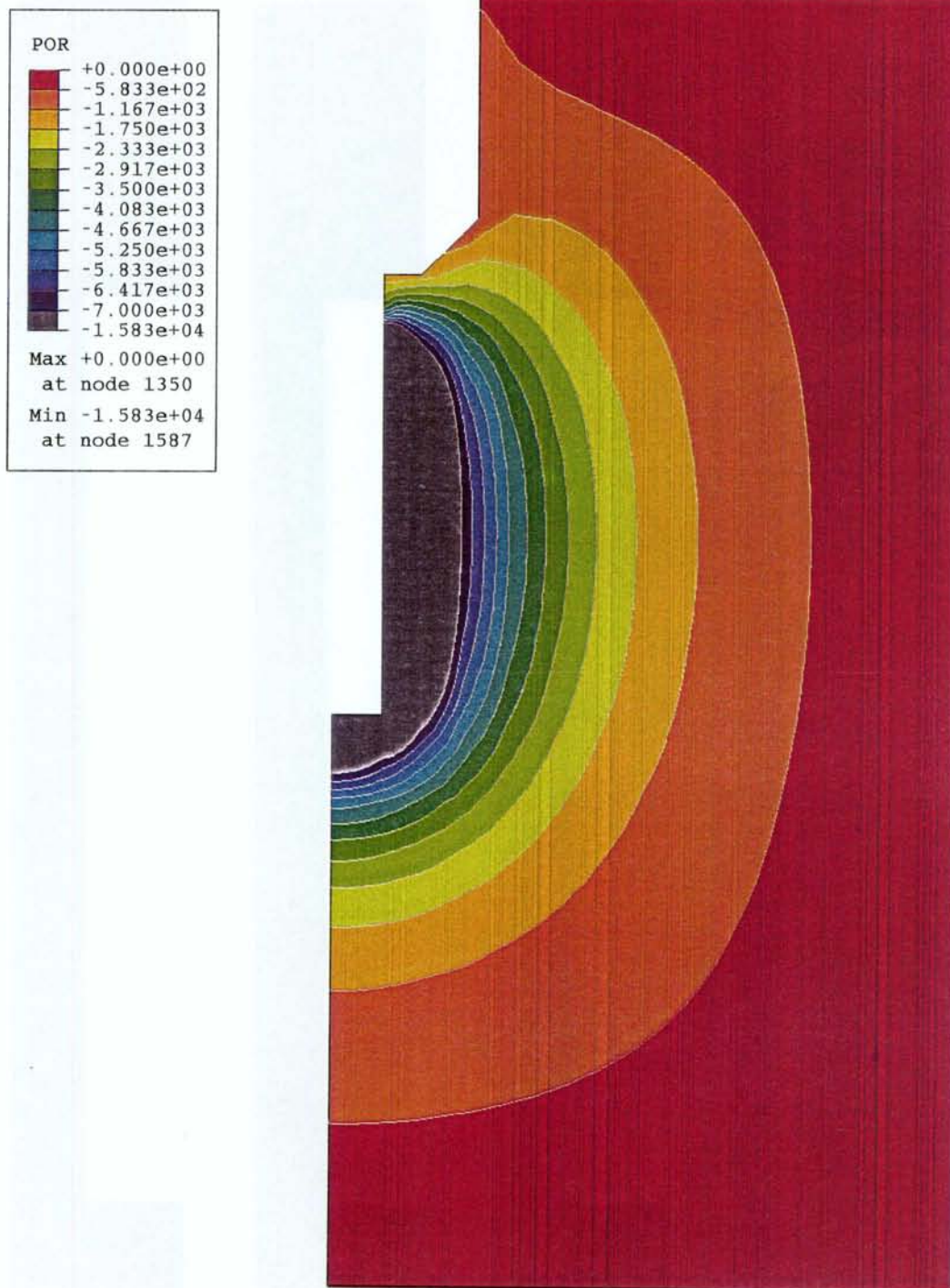
ODB: stress_2a.odb   ABAQUS/Standard 5.8-1   Mon Dec 14 17:14:07 CET

Figure 7-9. Calculation Stress_2a. Pore water pressure (kPa) in the rock after 8 years
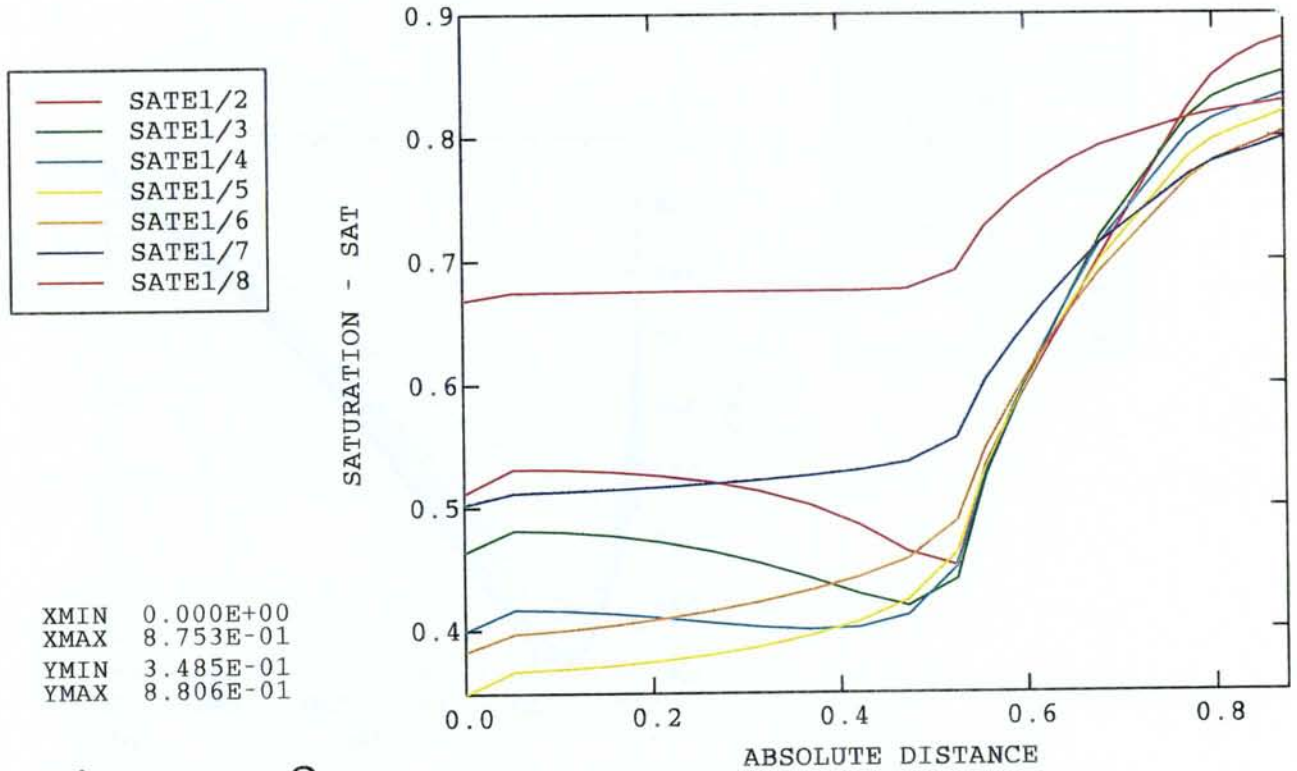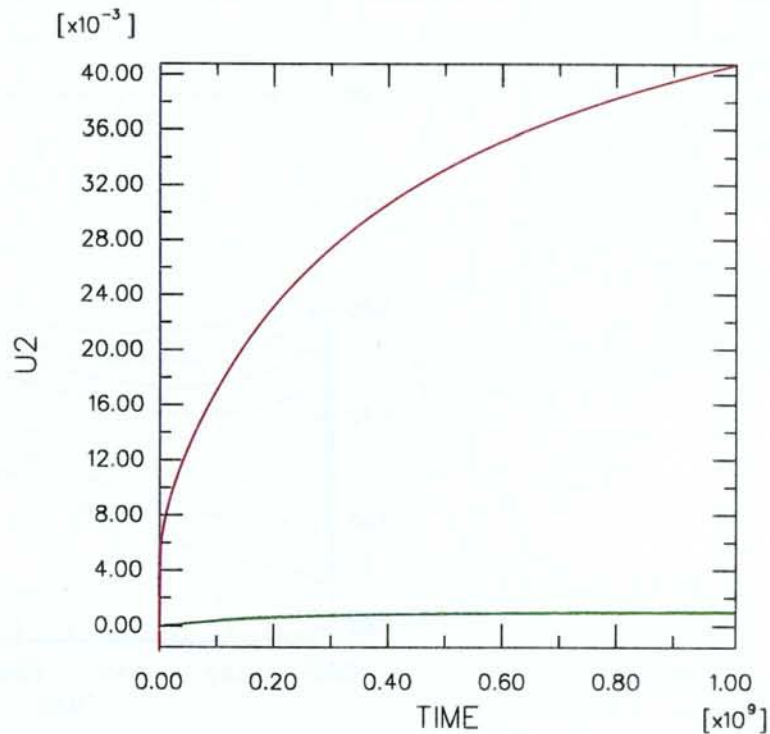
Figure 7-10. Calculation Stress_2a. Upper diagram: Degree of saturation as a function of the radial distance from the centre of the canister lid after 0.5 years (/2), 1.0 year (/3), 2.0 years (/4), 4.0 years (/5), 8.0 years (/6), 16.0 years (/7), and 32.0 years (/8) years. Lower diagram: Displacement (m) of the canister (red) and the centre of the boundary between the buffer and backfill (green) as a function of time (s)
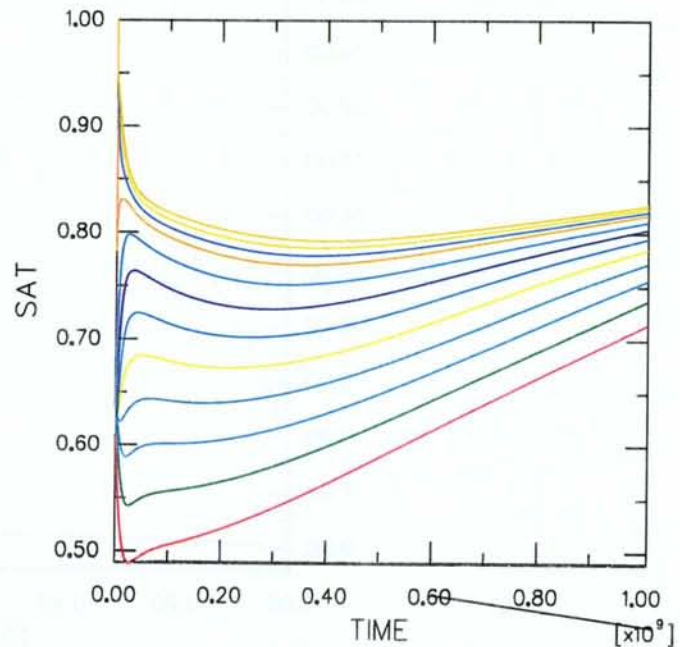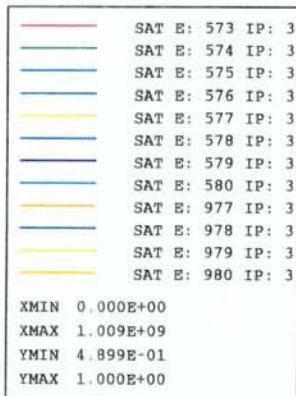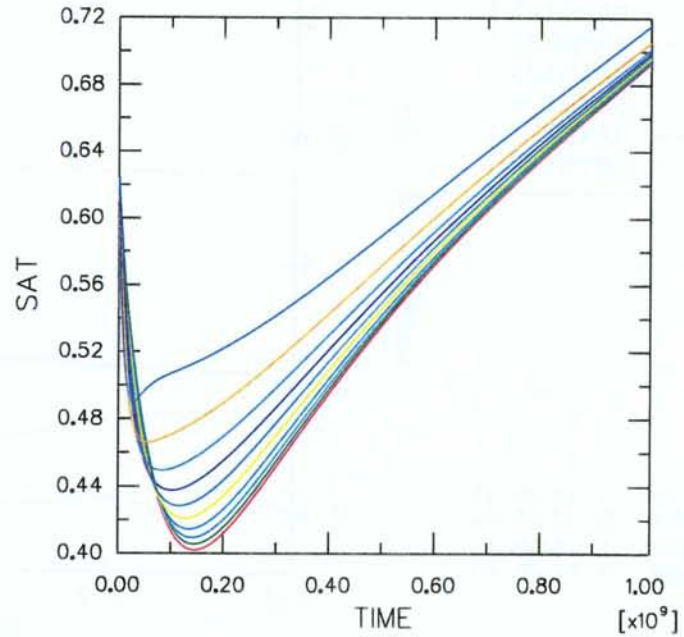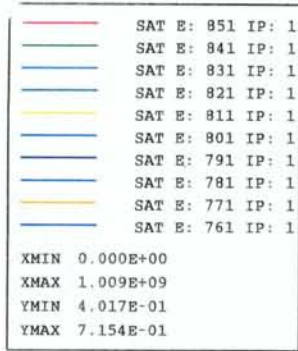
Figure 7-11. Calculation Stress_2a. The degree of saturation in the buffer of equidistant points along the radial line on top of the canister as a function of time (s). Upper: From 0 m to 0.525 m (along the canister lid). Lower: From 0.525 m to 0.875 m.

SAT
(Ave. Crit.: 100%)
+1.006e+00
+1.000e+00
+9.501e-01
+9.001e-01
+8.501e-01
+8.001e-01
+7.501e-01
+7.000e-01
+6.500e-01
+6.000e-01
+5.500e-01
+5.000e-01
+4.500e-01
+4.000e-01
Max +1.000e+00
 at elem 768 int 2
Min +6.048e-01
 at elem 851 int 3

ODB: stress_3b1.odb   ABAQUS/Standard 5.8-1   Mon Dec 14 23:29:41 CET
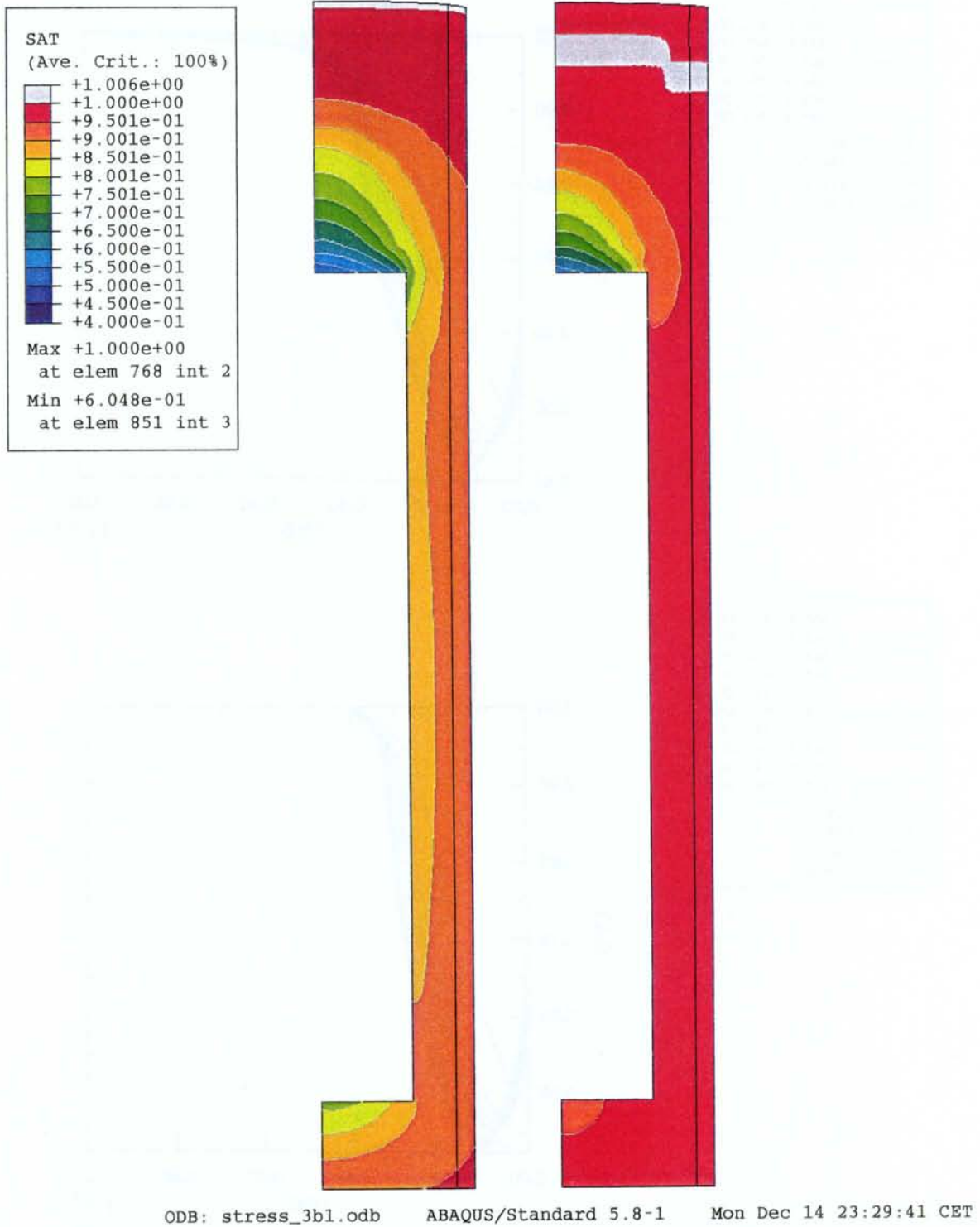
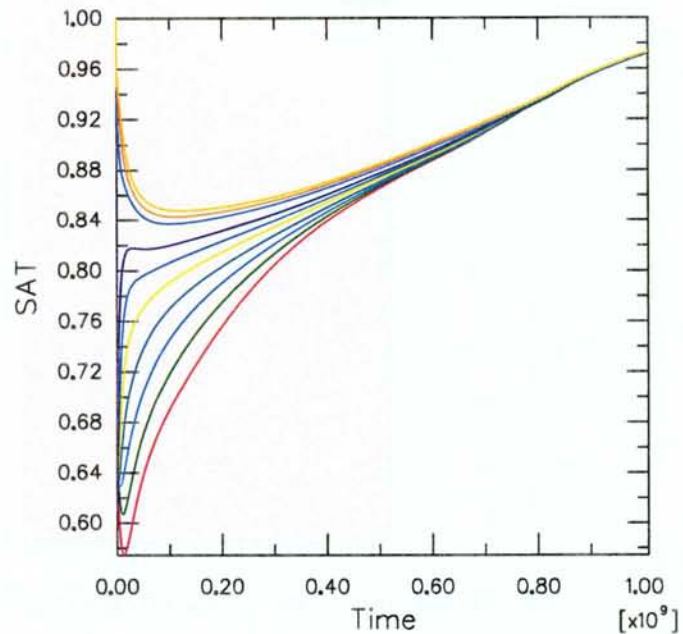*Figure 7-12. Calculations Stress_3a and 3b1. The degree of saturation after 8 years when the external water pressure is 0 (left) and 5 MPa.*
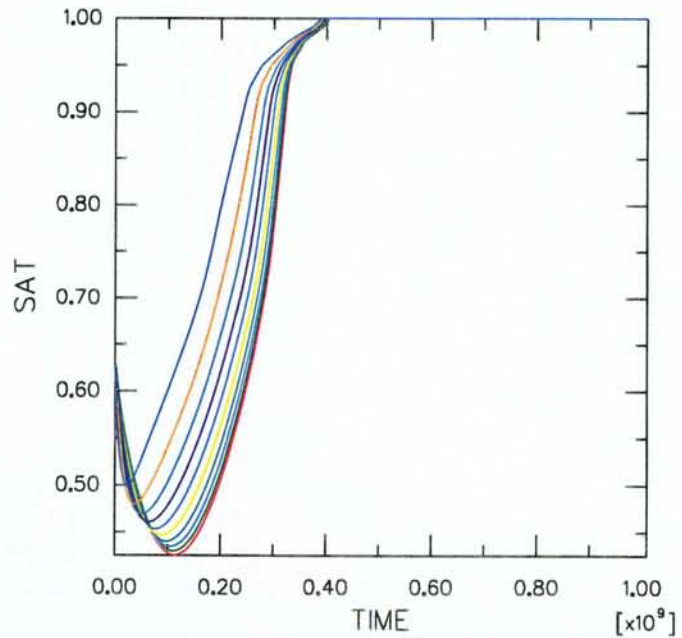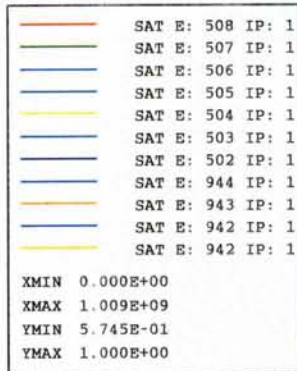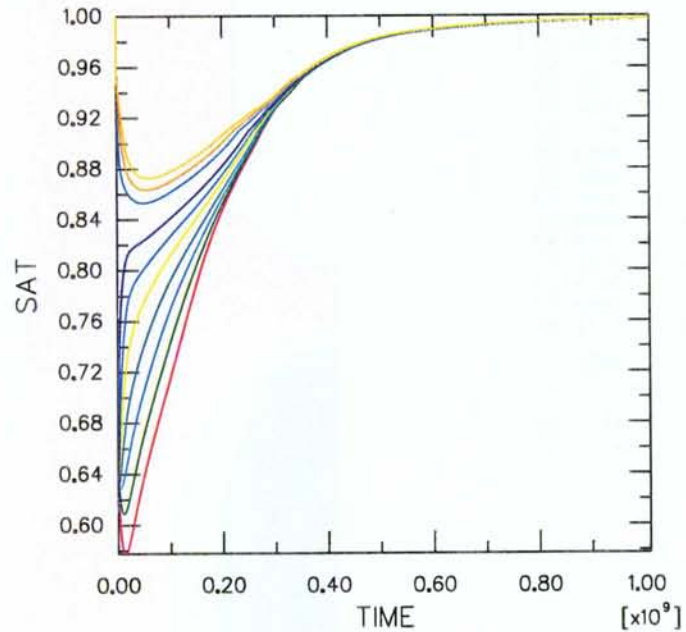
Figure 7-13. Calculations Stress_3a and 3b1. The degree of saturation in the buffer of equidistant points along the radial line on top of the canister as a function of time (s) when the external water pressure is 0 (upper) and 5 MPa.

ODB: stress_3b2_o.odb   ABAQUS/Standard 5.8-6   Thu Feb 04 05:04:51
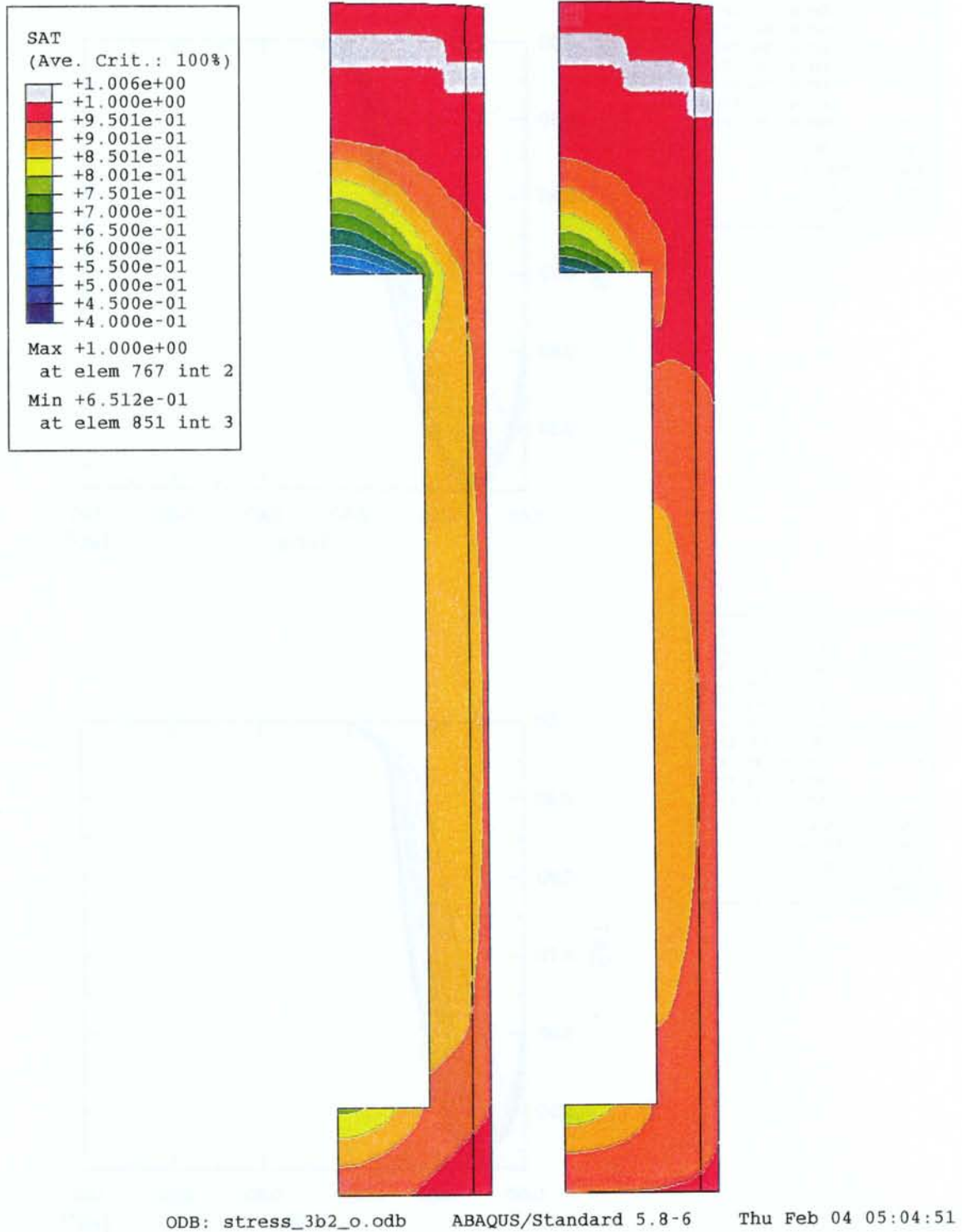
*Figure 7-14. Calculations Stress_3b1_o and 3b2_o. The degree of saturation after 8
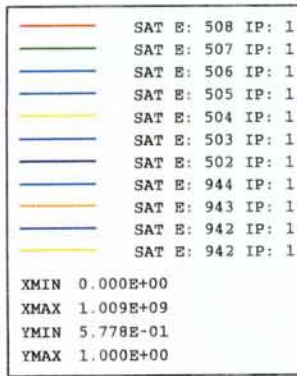years without damaged zone (left) and with damaged zone.*
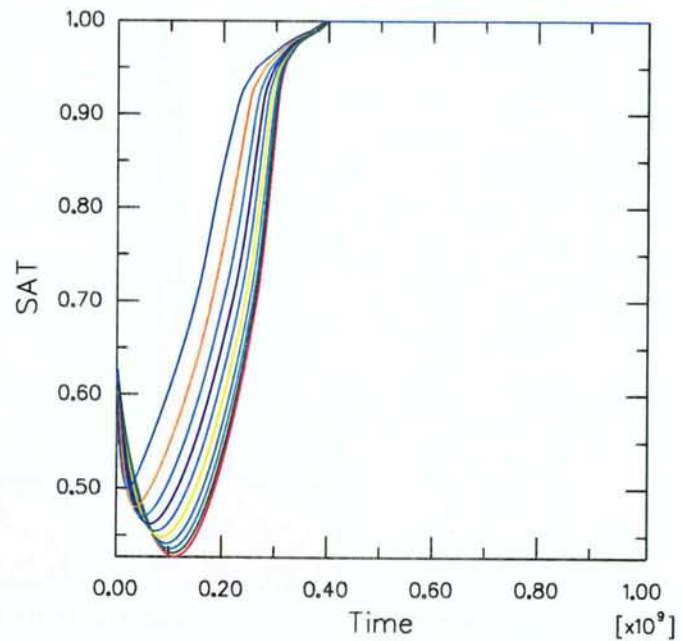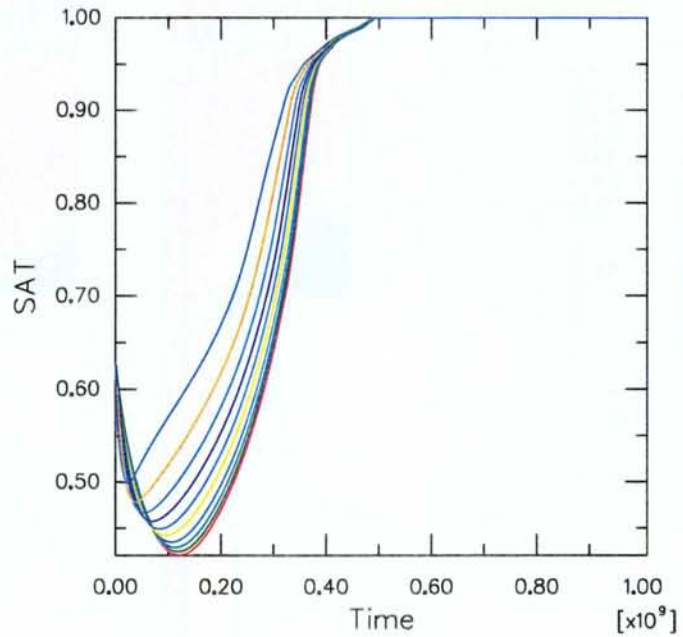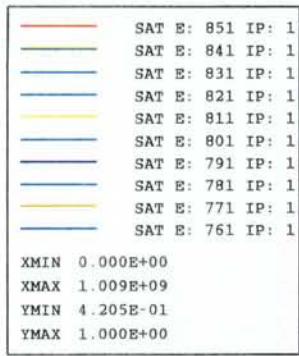
Figure 7-15. Calculations Stress_3b1_o and 3b2_o. The degree of saturation in the buffer of equidistant points along the radial line on top of the canister as a function of time (s) without damaged zone (upper) and with damaged zone.

ODB: stress2_3b2_o.odb   ABAQUS/Standard 5.8-6   Wed Feb 10 22:37:40

*Figure 7-16. Calculations Stress2_3b1_o and 2_3b2_o. The degree of saturation after 2
years without damaged zone (left) and with damaged zone.*

ODB: stress2_3b1_o.odb   ABAQUS/Standard 5.8-6   Wed Feb 03 03:41:28
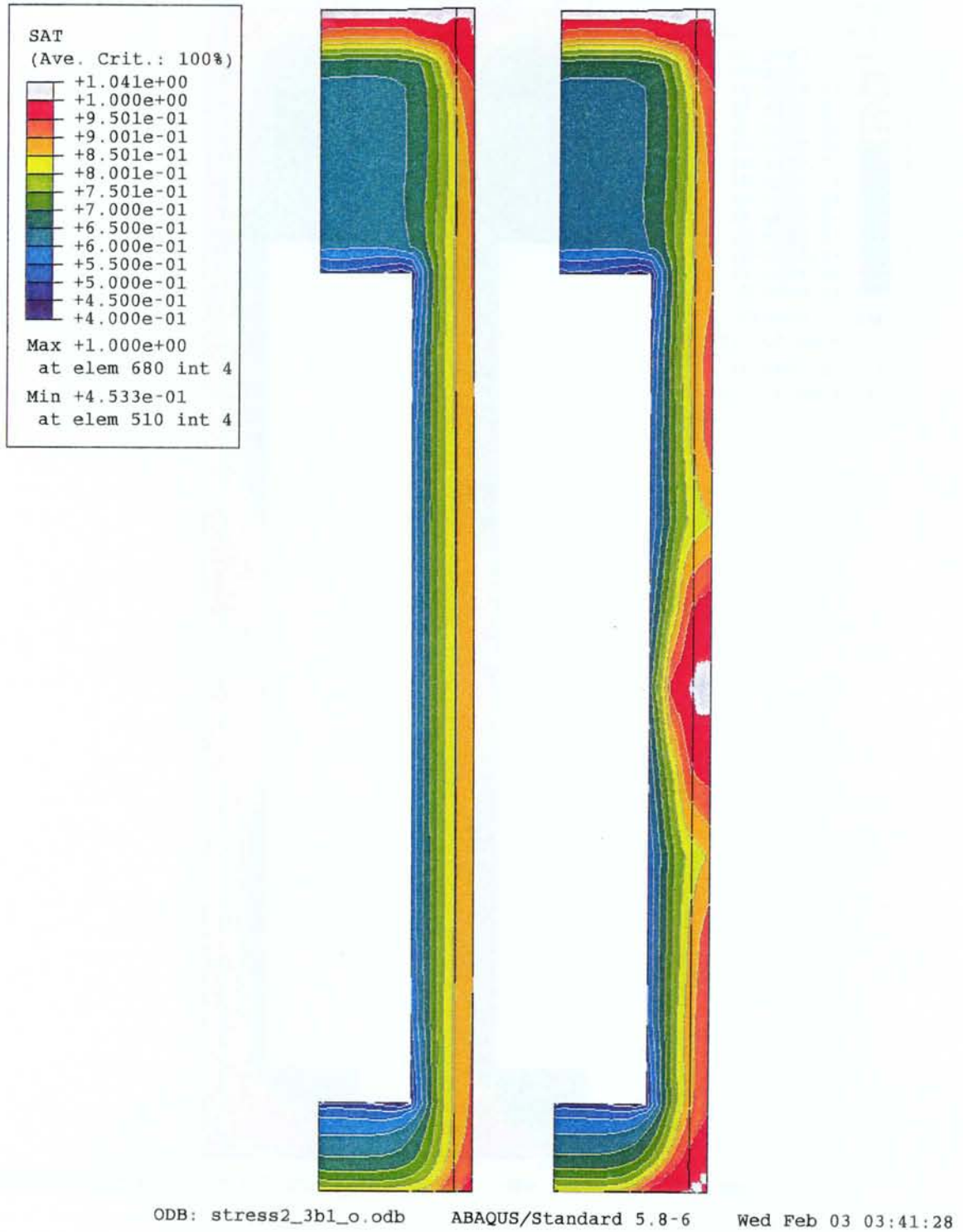
Figure 7-17. Calculations Stress_3b1_o and 2_3b1_o. Degree of saturation after 1 year without fractures (left) and with fractures.
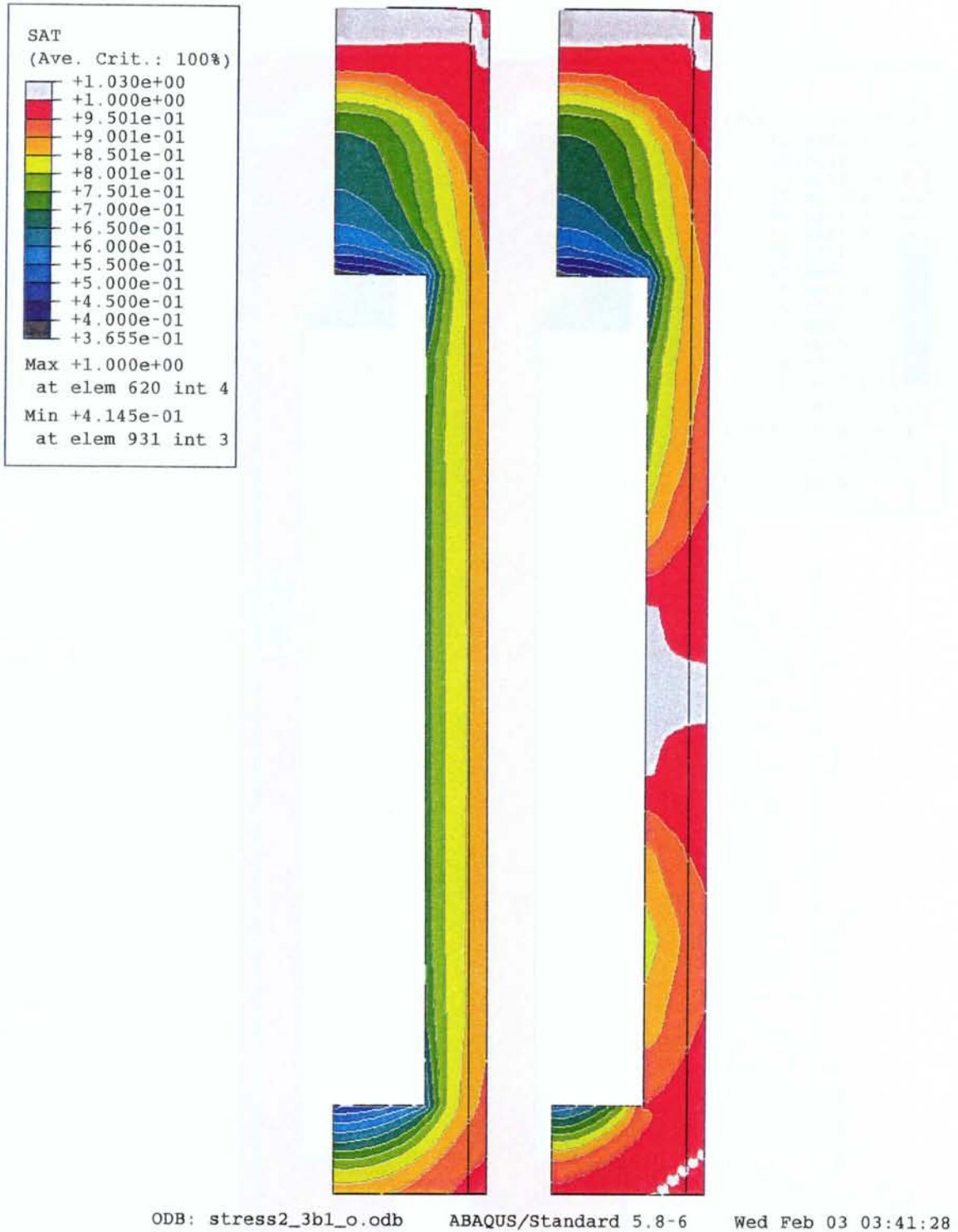
Figure 7-18. Calculations Stress_3b1_o and 2_3b1_o. Degree of saturation after 4 years without fractures (left) and with fractures.

SAT
(Ave. Crit.: 100%)
    +1.008e+00
    +1.000e+00
    +9.501e-01
    +9.001e-01
    +8.501e-01
    +8.001e-01
    +7.501e-01
    +7.000e-01
    +6.500e-01
    +6.000e-01
    +5.500e-01
    +5.000e-01
    +4.500e-01
    +4.000e-01
Max +1.000e+00
  at elem 501 int 1
Min +5.573e-01
  at elem 931 int 3
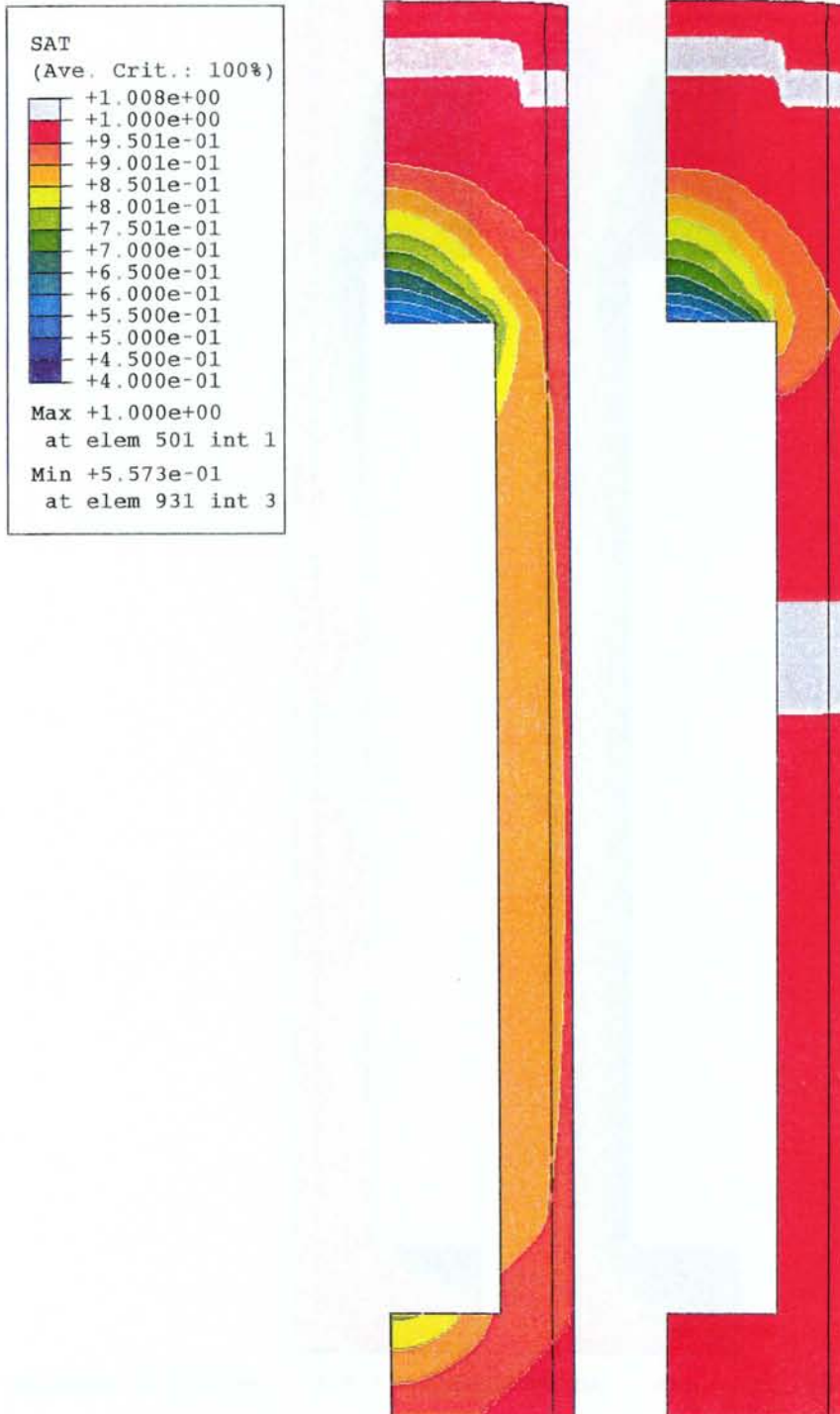
Figure 7-19. Calculations Stress_3b1_o and 2_3b1_o. Degree of saturation after 8 years without fractures (left) and with fractures.

ODB: stress_3b1_o.odb   ABAQUS/Standard 5.8-6   Sat Feb 06 02:49:02 CET

Figure 7-20. Calculations Stress_3b1_o and 2_3b1_o. Pore water pressure (kPa) in the rock after 4 years without fractures (left) and with fractures.
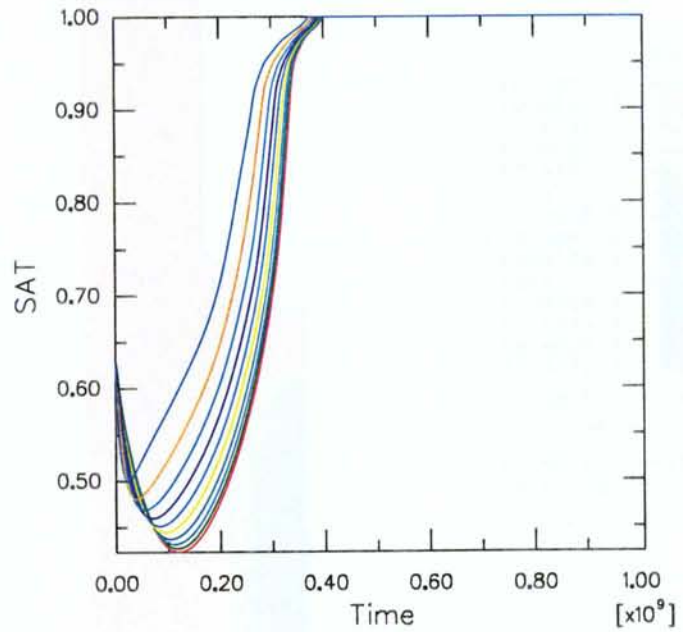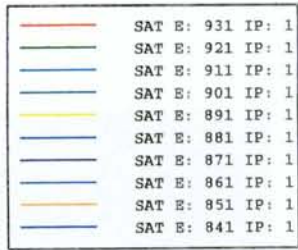
Figure 7-21. Calculations Stress_3a and 3a_o. The degree of saturation in the buffer of equidistant points along the radial line between the canister and the rock in the center of the canister as a function of time (s) without de-saturation (upper) and with de-saturation of the rock.

POR
+0.000e+00
-5.833e+02
-1.167e+03
-1.750e+03
-2.333e+03
-2.917e+03
-3.500e+03
-4.083e+03
-4.667e+03
-5.250e+03
-5.833e+03
-6.417e+03
-7.000e+03
-1.511e+04

Max +0.000e+00
at node 1350

Min -1.511e+04
at node 1729

ODB: stress_3a_o.odb   ABAQUS/Standard 5.8-6   Thu Feb 04 00:00:43 MET

Figure 7-22. Calculations Stress_3a and 3a_o. Pore water pressure (kPa) in the rock after 2 years with de-saturated rock (left) and without.
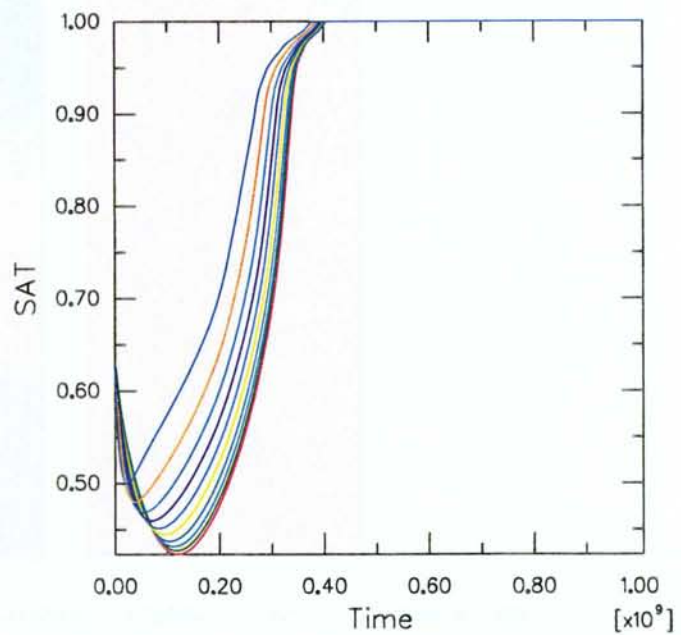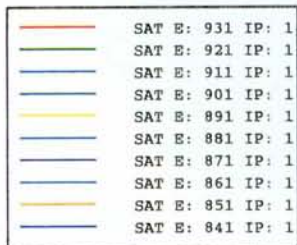
Figure 7-23. Calculations Stress2_3b1_oa and 2_3b1_ob. The degree of saturation in the buffer of equidistant points along the radial line between the canister and the rock in the centre of the canister as a function of time (s) with high permeable fractures (upper) and low permeable fractures..

SAT
(Ave. Crit.: 100%)
+1.041e+00
+1.000e+00
+9.501e-01
+9.001e-01
+8.501e-01
+8.001e-01
+7.501e-01
+7.000e-01
+6.500e-01
+6.000e-01
+5.500e-01
+5.000e-01
+4.500e-01
+4.000e-01
Max +1.000e+00
at elem 680 int 4
Min +4.523e-01
at elem 510 int 4

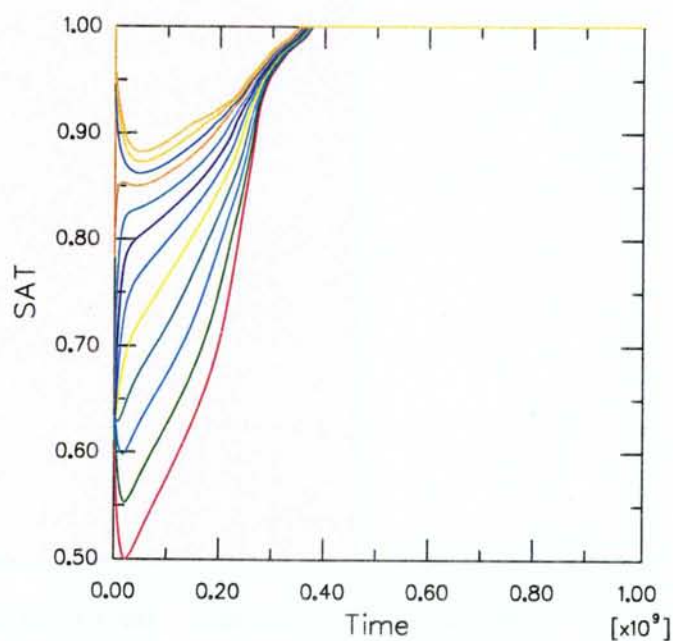ODB: stress2_3b1_ob.odb   ABAQUS/Standard 5.8-6   Sun Feb 07 20:23:54 C
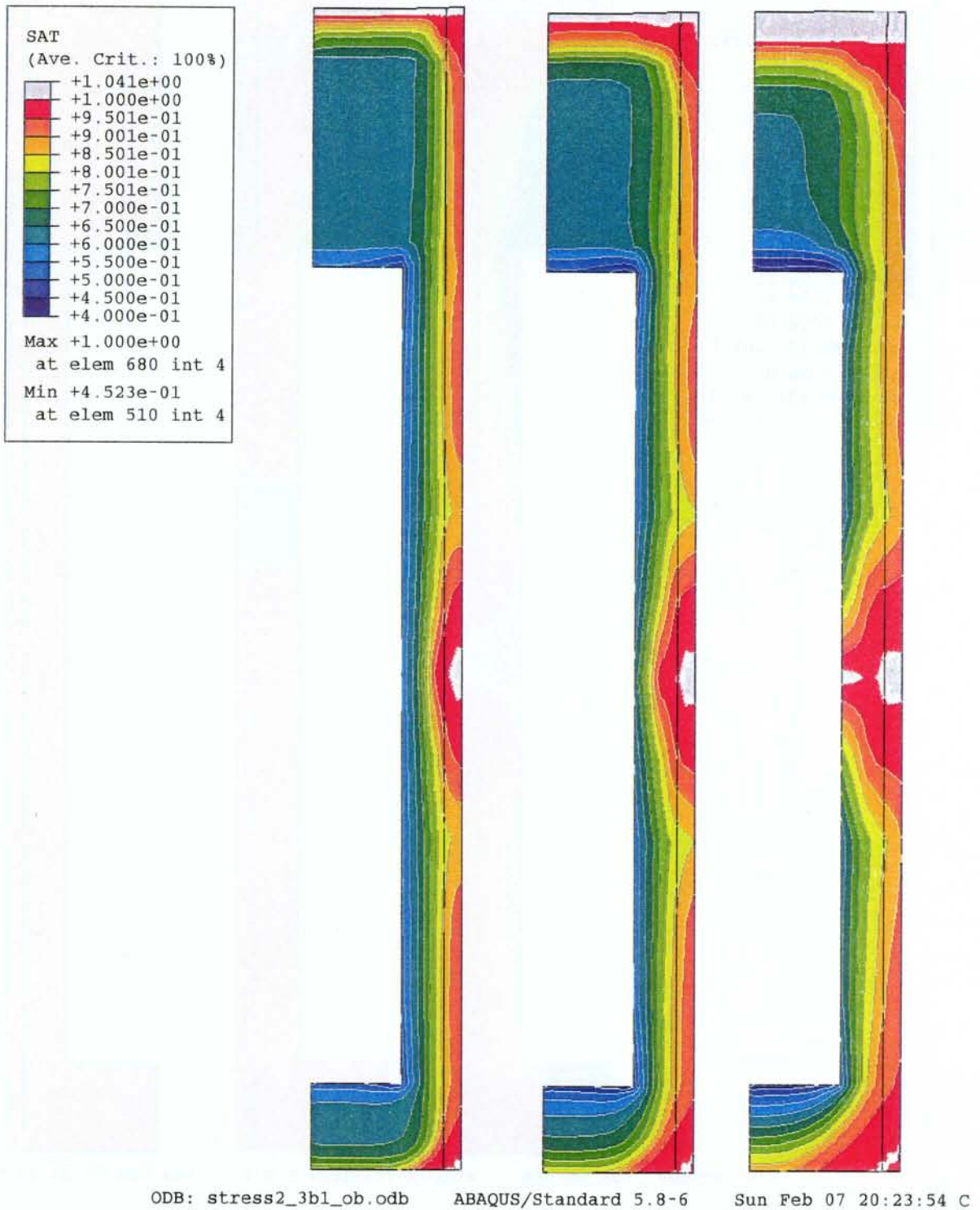
Figure 7-24. Calculation Stress2_3b1_ob. Degree of saturation after 0.5, 1.0, and 2.0 years (left to right)

ODB: stress2_3b1_ob.odb   ABAQUS/Standard 5.8-6   Sun Feb 07 20:23:54
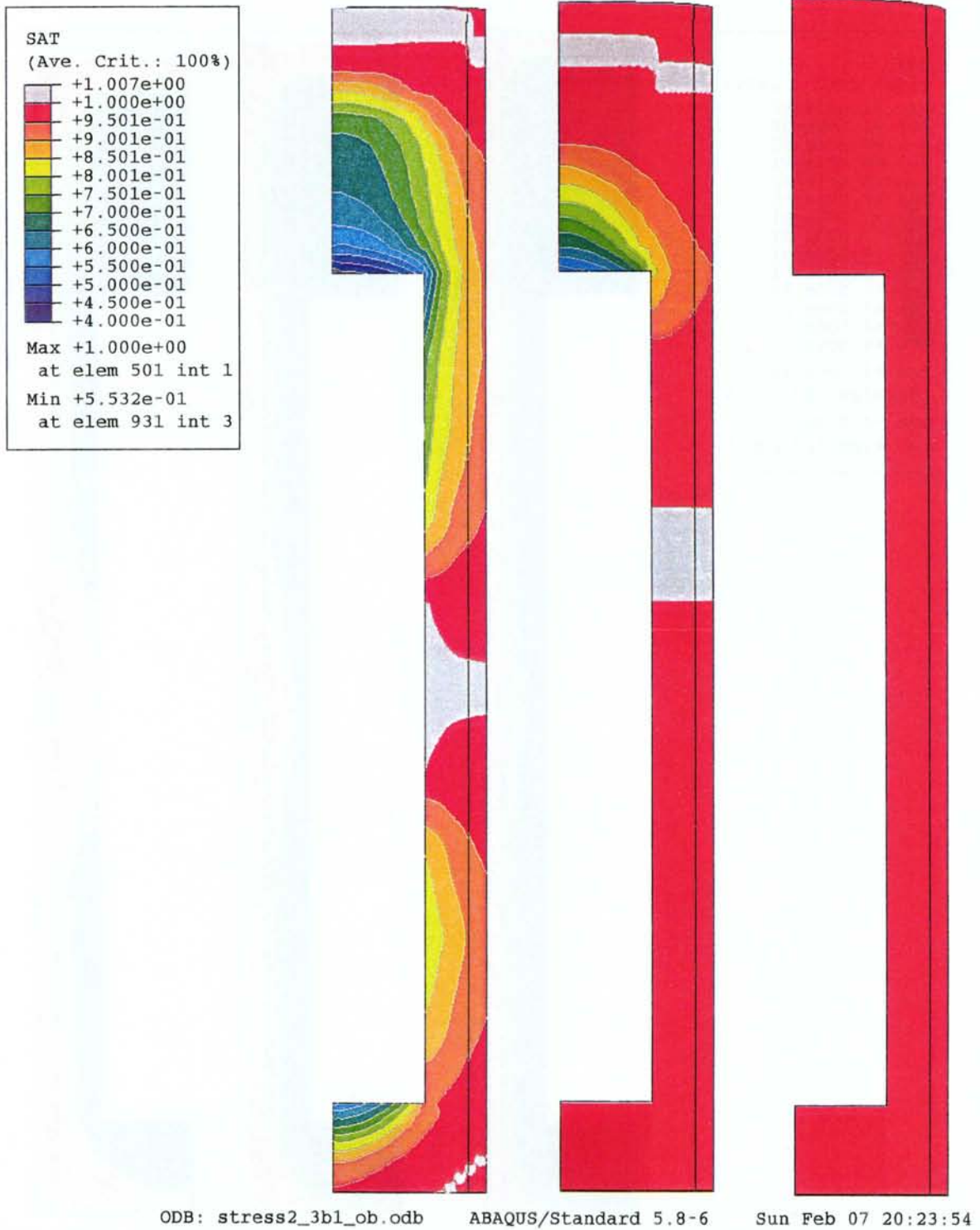
Figure 7-25. Calculation Stress2_3b1_ob. Degree of saturation after 4, 8, and 16 years (left to right)
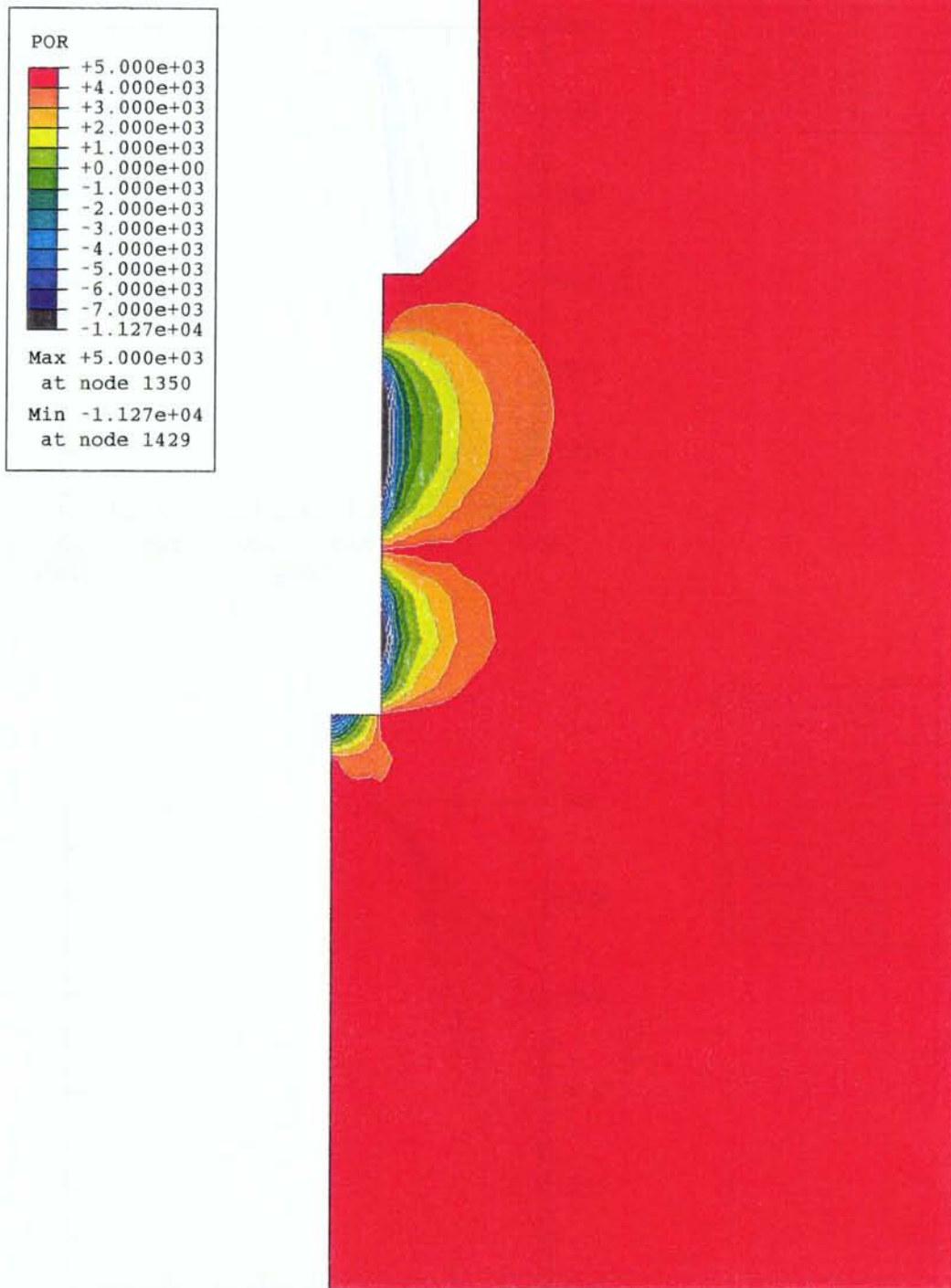
ODB: stress2_3b1_ob.odb   ABAQUS/Standard 5.8-6   Sun Feb 07 20:23:54

Figure 7-26. Calculations Stress2_3b1_ob. Pore water pressure (kPa) in the rock after 4 years. The rock is de-saturated at the grey, blue and dark green areas.
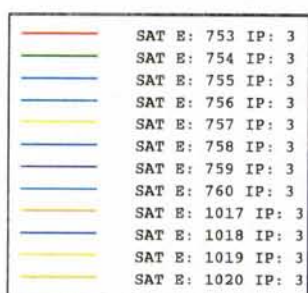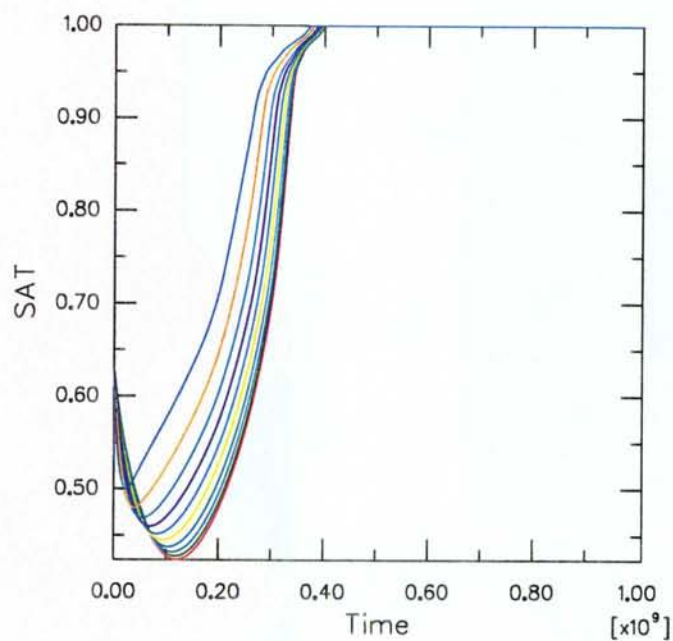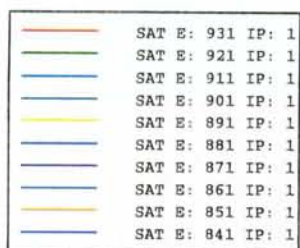
Figure 7-27. Calculation Stress2_3b1_ob. Degree of saturation in the buffer at equidistant points along the radial line on top of the canister as a function of time (s). Upper: From 0 m to 0.525 m (along the canister lid). Lower: From 0.525 m to 0.875 m.
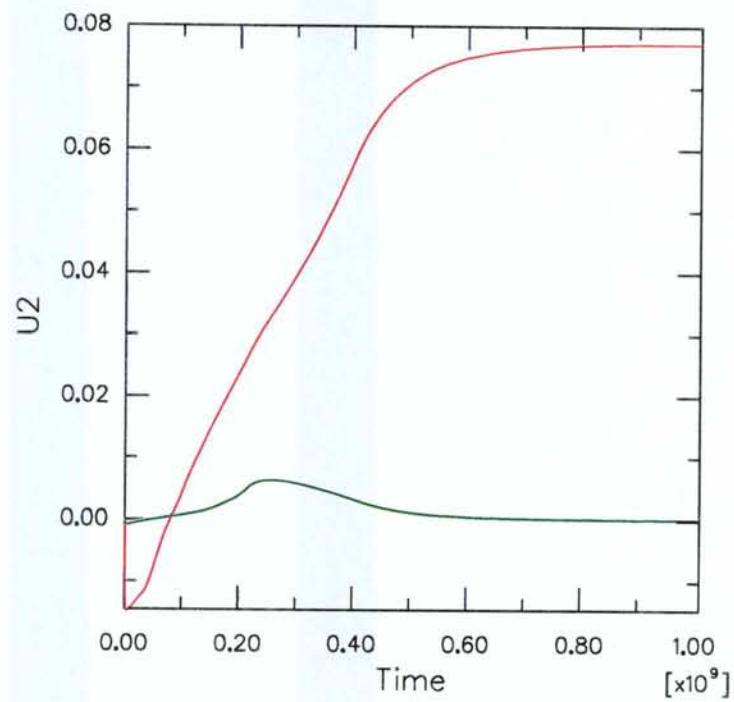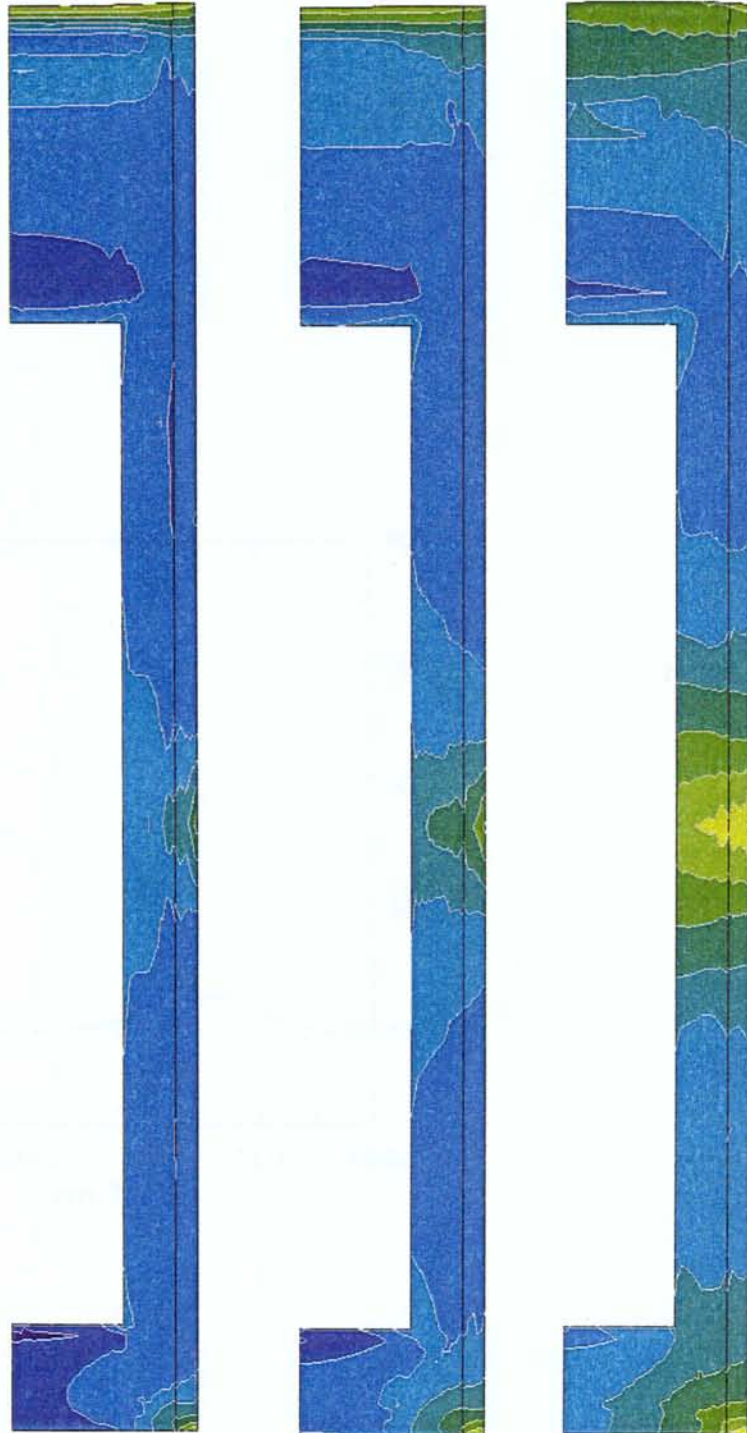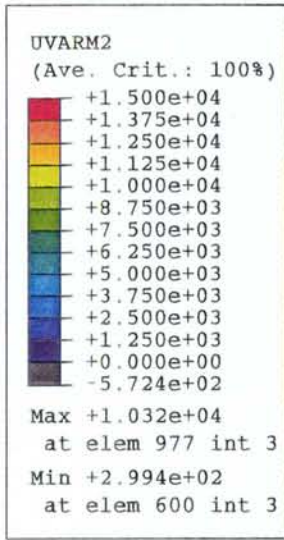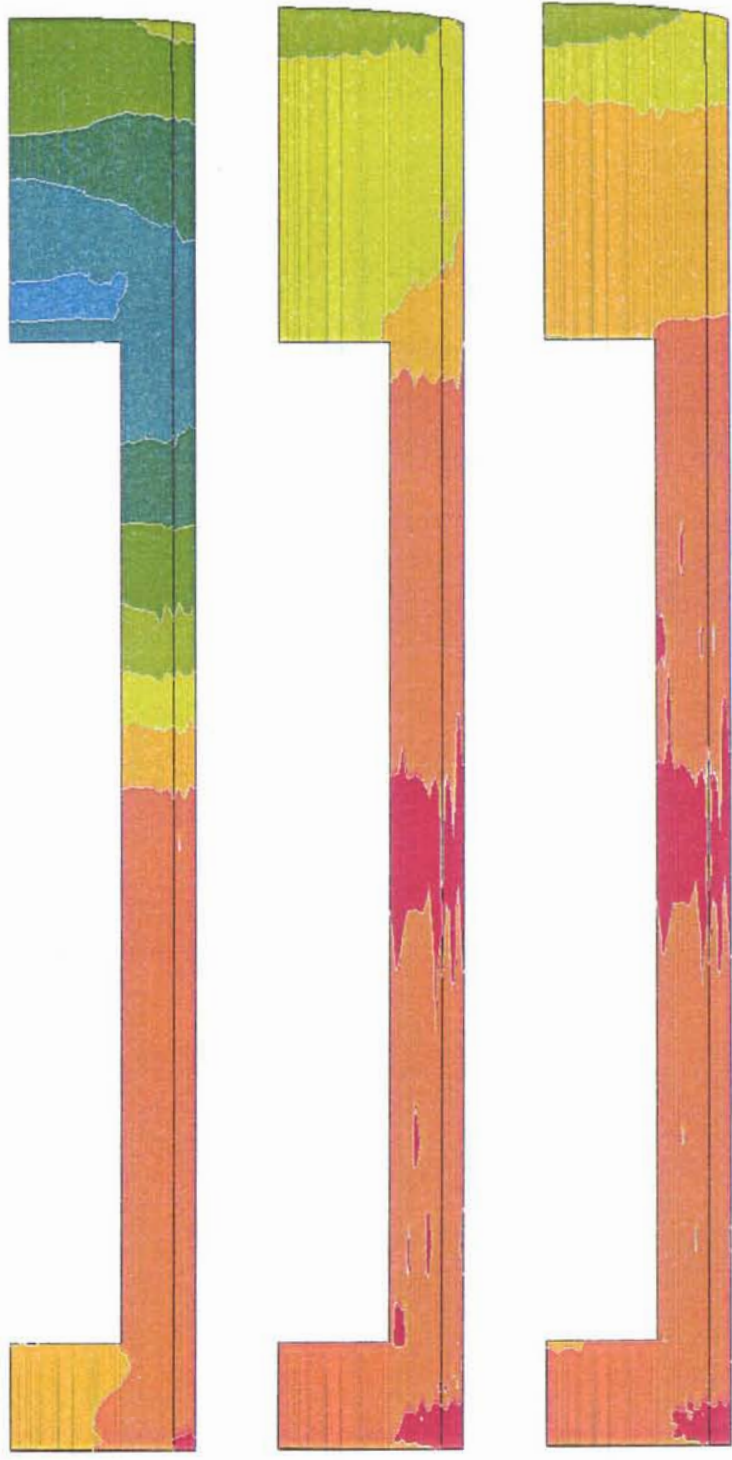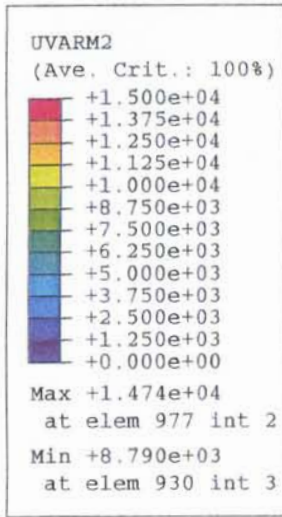
Figure 7-28. Calculation Stress2_3b1_ob. Displacement (m) of the canister (red) and the centre of the boundary between the buffer and backfill (green) as a function of time (s)

Figure 7-29. Calculation Stress2_3b1_ob. Radial total pressure after 1.0, 2.0, and 4.0 years (left to right)

UVARM2
(Ave. Crit.: 100%)
    +1.500e+04
    +1.375e+04
    +1.250e+04
    +1.125e+04
    +1.000e+04
    +8.750e+03
    +7.500e+03
    +6.250e+03
    +5.000e+03
    +3.750e+03
    +2.500e+03
    +1.250e+03
    +0.000e+00
Max +1.474e+04
  at elem 977 int 2
Min +8.790e+03
  at elem 930 int 3

ODB: stress2_3b1_ob.odb   ABAQUS/Standard 5.8-6   Wed Feb 10 22:40:04

Figure 7-30. Calculation Stress2_3b1_ob. Radial total pressure after 8, 16, and 32 years (left to right)